# Structure and tectonic evolution of the South Sandwich arc

ROBERT D. LARTER[1], LIEVE E. VANNESTE[1], PETER MORRIS[1] & DAVID K. SMYTHE[2,3]

[1]*British Antarctic Survey, High Cross, Madingley Road, Cambridge CB3 0ET, UK (e-mail: r.larter@bas.ac.uk)*

[2]*Department of Geology and Applied Geology, University of Glasgow, UK*

[3]*Present address: GeoLogica Ltd, 191Wilton Street, Glasgow G20 6DF, UK*

**Abstract:** Detailed analysis of marine magnetic profiles from the western part of the East Scotia Sea confirms continuous, organized back-arc spreading since at least 15 Ma ago. In the eastern part of the East Scotia Sea, the South Sandwich arc lies on crust that formed at the back-arc spreading centre since 10 Ma ago, so older back-arc crust forms the basement of the present inner forearc. Interpretations of two multichannel seismic reflection profiles reveal the main structural components of the arc at shallow depth, including evidence of trench-normal extension in the mid-forearc, and other features consistent with ongoing subduction erosion. The seismic profile interpretations have been used to constrain simple two-dimensional gravity models. The models were designed to provide constraints on the maximum possible thickness of the arc crust, and it is concluded that this is 20 and 19.2 km on the northern and southern lines, respectively. On the northern line the models indicate that the forearc crust cannot be much thicker than normal oceanic crust. Even with such thin crust, however, the magmatic growth rate implied by the cross-section of the arc crust is within the range recently estimated for two other arcs that have been built over a much longer interval.

The South Sandwich island arc is a classic intra-oceanic arc in the southernmost Atlantic Ocean (Fig. 1). The arc is situated on the small Sandwich Plate, which is overriding the southernmost part of the South American Plate at the South Sandwich Trench at a rate of 67–81 mm $a^{-1}$ (Pelayo & Wiens 1989; Thomas *et al.* 2003) (Fig. 1). Further west, the Sandwich Plate is separating from the Scotia Plate at the East Scotia Ridge (ESR) back-arc spreading centre, where the full spreading rate is 60–70 mm $a^{-1}$ (Thomas *et al.* 2003).

Early studies of marine magnetic profiles from the East Scotia Sea showed that E–W back-arc spreading had been active since at least 8 Ma ago (Barker 1970, 1972; Barker & Hill 1981). More recently Barker (1995) identified lineated magnetic anomalies out to at least anomaly 5 (9.7–10.9 Ma) and probably out to anomaly 5B (*c.* 15 Ma) on the western flank of the ESR. On the eastern flank of the ESR, the central part of the South Sandwich island arc lies on crust formed at the ESR during anomaly 5. Therefore, the identification of anomalies older than anomaly 5, if confirmed, has important implications for the tectonic evolution of the arc and can provide a basis for quantitative estimates of rates of processes such as sediment subduction and subduction erosion (Vanneste & Larter 2002).

In this paper we present a detailed analysis of new and archive magnetic profiles across the western margin of the East Scotia Sea, confirming that organized back-arc spreading has been active since at least 15 Ma ago. We speculate that spreading was probably preceded by a phase of arc rifting, as observed in other back-arc basins (e.g. Parson & Hawkins 1994; Martinez *et al.* 1995; Baker *et al.* 1996; Parson & Wright 1996), and that rifting was triggered by a change in South American–Antarctic plate motion about 20 Ma ago. We also present interpretations of two multichannel seismic (MCS) reflection profiles that cross the trench, arc and ESR, and use these to constrain two-dimensional gravity models. Implications of the MCS interpretations and gravity modelling results are discussed in the context of the confirmed history of >15 Ma of continuous, organized back-arc spreading.

## Marine magnetic record of back-arc spreading

Marine magnetic profiles were examined to constrain the time of onset and early history of back-arc spreading in the East Scotia Sea. Several long profiles were selected for analysis, including eight that cross the oldest back-arc crust at the western limit of the East Scotia Sea

*From:* LARTER, R.D. & LEAT, P.T. 2003. *Intra-Oceanic Subduction Systems: Tectonic and Magmatic Processes.* Geological Society, London, Special Publications, **219**, 255–284. 0305-8719/03/$15.00

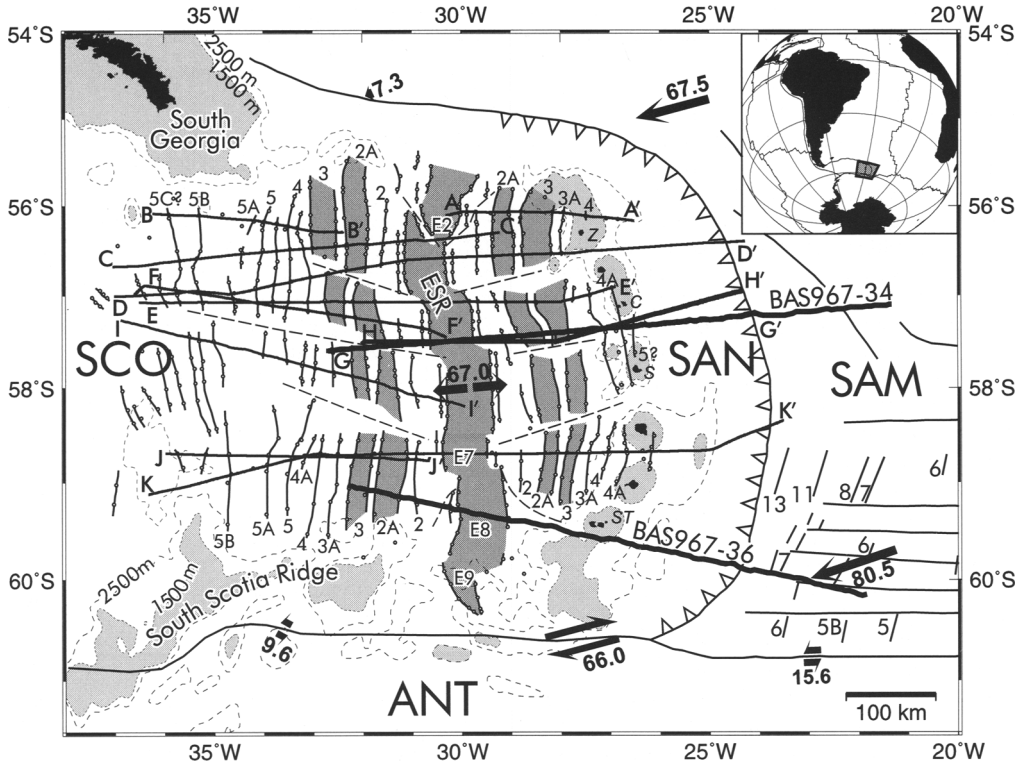


**Fig. 1.** Location map showing the tectonic setting of the South Sandwich island arc, and marine magnetic anomalies in the East Scotia Sea, modified from Vanneste *et al.* (2002). The grey-filled box on the globe in the inset shows the location of the main map. Magnetic anomaly picks are represented by small open circles. The central Brunhes anomaly and anomalies 2A and 3 are shaded dark grey. Segments E2 and E7–E9 of the East Scotia Ridge (ESR) are labelled. Long-dashed lines represent pseudofaults formed by ridge-segment propagation (Livermore *et al.* 1994, 1997). Magnetic anomaly identifications on the South American Plate are based on Barker & Lawver (1988). Arrows indicate vectors of relative motion between the Scotia (SCO), Sandwich (SAN), South American (SAM) and Antarctic (ANT) plates, based on Euler vectors of Thomas *et al.* (2003). Arrow lengths are proportional to rates (annotated in mm $a^{-1}$). Locations of magnetic and bathymetry profiles A–A′ to K–K′ that are shown in Figure 2 and 3 are shown as solid lines. Locations of Sandwich Lithospheric and Crustal Experiment (SLICE) multichannel seismic lines BAS967-34 and BAS967-36 are shown as thicker black lines. The 2500 m (short-dashed lines) and 1500 m (filled, light grey) bathymetric contours, based on global seafloor topography data of Smith & Sandwell (1997), define the South Sandwich arc, South Georgia microcontinental block and South Scotia Ridge. The barbed line represents the trench. Island labels (italics): C, Candlemas Island; S, Saunders Island; ST, Southern Thule; Z, Zavodovski Island.

(Fig. 1). In previous interpretations of East Scotia Sea spreading history the existence of long, approximately E–W-trending fracture zones was inferred (Barker & Hill 1981; Barker 1995). However, a swath sonar investigation of the entire ESR revealed no stable fracture zone offsets (Livermore *et al.* 1995, 1997; Bruguier & Livermore 2001), and therefore we consider it likely that the prominent WNW–ESE-trending gravity anomalies in the western part of the East Scotia Sea (Livermore *et al.* 1994) represent the loci of migrating ridge offsets (i.e. pseudofaults). Some magnetic profiles used in previous interpretations of East Scotia Sea spreading history probably included unrecognized offsets across these pseudofaults. Magnetic lineations between pseudofaults trend N–S, and it is likely that the extension direction has been approximately E–W throughout the development of the East Scotia Sea.

In selecting magnetic profiles for analysis of spreading rates we gave priority to those that avoid crossing pseudofaults. After removal of the International Geomagnetic Reference Field

(IGRF; Barton 1996), the selected profiles were projected onto E–W lines and compared to synthetic magnetic anomaly profiles to identify anomalies (Fig. 2). Six of the 11 profiles shown in Figure 2 were collected during cruises in 1995 and 1997, and thus were not included in the analysis of Barker (1995). The geomagnetic polarity timescale of Cande & Kent (1995) was used in the generation of the synthetic magnetic anomaly profiles, and is the basis for all magnetic anomaly ages quoted in this paper. Initial identifications of anomalies were made by comparison with a set of synthetic profiles generated using a range of constant spreading rates. The variable spreading rates used to generate the synthetic profiles shown in Figure 2 were based on reduced distance analyses (see below).

Six of the eight profiles that extend to the western limit of the East Scotia Sea show a pair of positive anomalies that are a very close match to anomalies 5AC and 5AD (13.9 and 14.4 Ma, respectively) on the synthetic profiles. Anomaly 5B (15.0 Ma) is a subtle feature on the synthetic profiles, but also appears to be present on several of the observed profiles. A little further west, another positive anomaly is observed on most of these profiles and is in approximately the position where anomaly 5C (16.4 Ma) would be expected to occur, given a constant spreading rate. However, to the west of this anomaly magnetic profiles are less consistent, so identification of it as 5C must remain tentative. Sharp offsets in seafloor depth occur near to this anomaly on several of the profiles (Fig. 3), perhaps indicating that it approximates the limit of back-arc crust formed by organized seafloor spreading.

On the eastern side of the back-arc basin, the crest of the northern end of the modern arc is approximately coincident with anomaly 4 (e.g. profiles A–A′ and D–D′ in Fig. 2), while the central part of the arc is approximately coincident with anomaly 5 (e.g. profiles G–G′, H–H′ and K–K′). Therefore, if an arc existed between 15 Ma ago and chron 5 (9.7–10.9 Ma), it must have been located farther east relative to the Sandwich Plate.

The interpretation of magnetic anomalies on the eastern side of the back-arc basin north of about 57°S, shown in Figures 1 and 2, is slightly different from that recently published in Vanneste & Larter (2002) and Vanneste *et al.* (2002). The revised interpretation results from careful comparison of the profiles in Figure 2 with synthetic profiles and consideration of reduced distance analyses (see below). In our revised interpretation, anomaly 3n in this part of the back-arc basin is wider than it was in the earlier interpretation, and we now think that the positive anomaly previously interpreted as 3An (6.2 Ma) is actually 3n.4n (5.1 Ma). This change also implies that the anomalies previously interpreted as 4n and 4An (7.9 and 8.9 Ma) on profiles in this area are actually 3An and 4n, respectively.

In general, there is a close correspondence between the observed magnetic profiles and the synthetic profiles in Figure 2. This close correspondence, and the continuity of the reversal sequence on the observed profiles, shows that the greater width of the western side of the East Scotia Sea compared to its eastern side cannot be attributed to ridge jumps. The crust formed on the eastern flank of the ESR prior to chron 5 must now lie beneath the inner forearc. Our analysis of spreading rates (see below) shows that the half spreading rates between chrons 5B and 5r (15.0–11.5 Ma) on the western side of the ESR were 17–20 mm $a^{-1}$, decreasing to 12–14 mm $a^{-1}$ during chrons 5r and 5n (11.5–10.0 Ma). If spreading during this interval was symmetrical, then the crust formed on the eastern flank of the ESR during chron 5B now lies about 80 km east of the central part of the present arc.

Studies in other back-arc basins have shown that the earliest stages of back-arc extension typically involve asymmetrical rifting and that a spreading axis tends to develop near, or propagate into, the trenchward flank of the rifted crust (Parson & Hawkins 1994; Martinez *et al.* 1995; Parson & Wright 1996). Furthermore, it has been suggested that magnetic lineations may be developed even in the rifting phase by systematic migration of zones of magmatism across the rift zone (Martinez *et al.* 1995). However, the asymmetrical extension described in these studies occurs during the arc-rifting phase that precedes organized back-arc spreading. The close correspondence between the observed magnetic profiles and the synthetic profiles shown in Figure 2, and the continuity of magnetic lineations along strike, leaves little doubt that extension in the East Scotia Sea had already progressed to organized spreading by 15 Ma ago. Even if it is assumed that quite extreme asymmetrical extension persisted into the spreading phase, with the western flank of the ESR spreading twice as fast as the eastern flank until 10 Ma ago, the crust formed on the eastern flank during chron 5B still must lie 40 km or more east of the central part of the present arc. As the present arc–trench gap is only 140–160 km, this implies that either spreading began unusually close to the trench or a substantial amount of subduction erosion has taken place.

Figure 4 shows the magnetic anomaly interpretation from Figure 1 overlaid on the

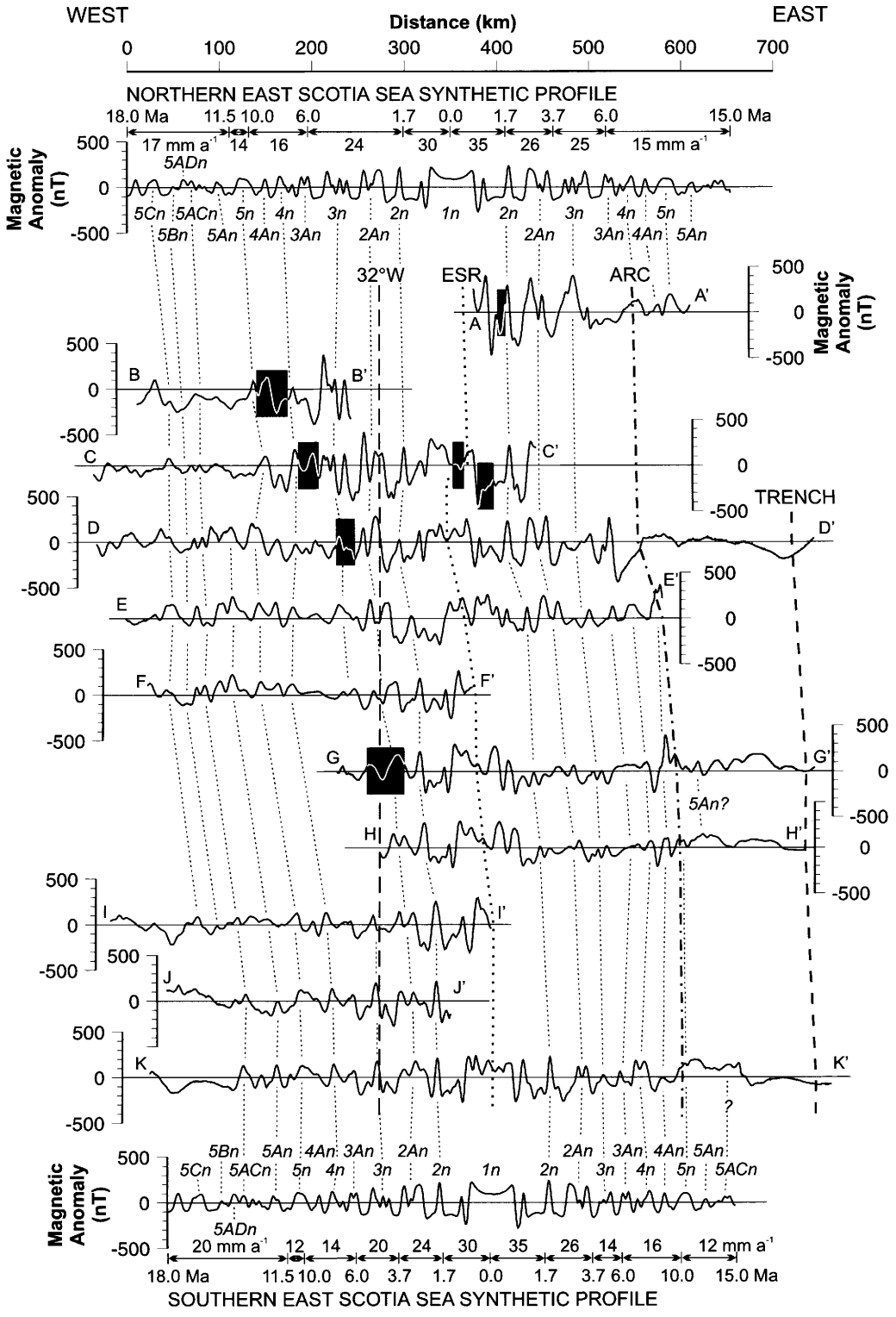
WEST
Distance (km)
EAST
0 100 200 300 400 500 600 700
NORTHERN EAST SCOTIA SEA SYNTHETIC PROFILE
18.0 Ma 11.5 10.0 6.0 1.7 0.0 1.7 3.7 6.0 15.0 Ma
17 mm a-1 14 16 24 30 35 26 25 15 mm a-1
Magnetic Anomaly (nT)
500
0
-500
5ADn
5Cn 5ACn 5n 4n 3n 2n 1n 2n 3n 4n 5n
5Bn 5An 4An 3An 2An 2An 3An 4An 5An
32°W
ESR
ARC
A
A'
B
B'
C
C'
TRENCH
D
D'
E
E'
F
F'
G
G'
5An?
H
H'
I
I'
J
J'
K
K'
?
5Bn 5An 4An 3An 2An 2An 3An 4An 5An
5Cn 5ACn 5n 4n 3n 2n 1n 2n 3n 4n 5n 5ACn
5ADn
20 mm a-1 12 14 20 24 30 35 26 14 16 12 mm a-1
18.0 Ma 11.5 10.0 6.0 3.7 1.7 0.0 1.7 3.7 6.0 10.0 15.0 Ma
SOUTHERN EAST SCOTIA SEA SYNTHETIC PROFILE

regional magnetic anomaly field. The regional field was calculated by subtracting the IGRF from all available marine magnetic profiles, carrying out cross-over error analysis on data from different cruises and sections of cruises (cruise files were subdivided where there was a significant break in data acquisition), applying constant corrections to data from each cruise section and then gridding the corrected anomaly data. Figure 4 confirms that most of our magnetic anomaly picks are on the peaks or edges of lineated magnetic anomalies, and also shows that lineated anomalies are present as far west as, and even beyond, the position where we have identified anomaly 5B. Furthermore, Figure 4 confirms that the interpreted pseudofaults correspond to discontinuities in the lineated magnetic anomalies.

The close correspondence between the observed and synthetic magnetic profiles in Figure 2 permits detailed analysis of spreading rates using the enhanced sensitivity of the reduced distance method (Barker 1979). On a reduced distance graph the distance along a profile at which a particular peak, trough or zero crossing is observed is shown after subtraction of the distance at which it occurs along a synthetic magnetic profile generated using a constant spreading rate, and the resulting value is plotted versus age. A spreading rate matching that of the synthetic profile would produce a horizontal line on a reduced distance graph, and this form of display is more sensitive to variations in spreading rate than a simple plot of distance v. time. The sensitivity of a reduced distance graph is greatest at spreading rates close to those of the reference synthetic profile.

Barker (1995) published reduced distance graphs based on comparison of six East Scotia Sea magnetic profiles with a synthetic profile generated using a constant half spreading rate of 25 mm $a^{-1}$. These graphs indicated that half spreading rates prior to 4 Ma averaged about 15 mm $a^{-1}$. In order to examine the early history of East Scotia Sea spreading in more detail we have plotted reduced distance graphs based on comparison of the projected profiles shown in Figure 2 with a synthetic profile generated using a constant half spreading rate of 15 mm $a^{-1}$ (Fig. 5). The distances on which these graphs are based were measured from a confidently identified peak or trough, rather than from the spreading axis. As it is the gradient of the graph that represents spreading rate, absolute values of reduced distance are unimportant.

The overall positive gradients on the reduced distance graphs in Figure 5 indicate that half spreading rates prior to 4 Ma averaged more than 15 mm $a^{-1}$. The graphs also reveal some significant N–S and temporal variations. Between 15 and 11.5 Ma ago half rates on the western flank of the ESR (Fig. 5a, b) were slightly slower on the northern (17 mm $a^{-1}$) than on the central and southern parts of the ridge (20 mm $a^{-1}$). About 11.5 Ma ago spreading rates along the whole ridge slowed abruptly, and from then until 4 Ma ago spreading at the northern part of the ESR was faster than at its central and

**Fig. 2.** Selected East Scotia Sea marine magnetic profiles compared to synthetic magnetic anomaly profiles. Locations of profiles A–A′ to K–K′ are shown in Figure 1. All of the profiles are projected on to 090° . The observed magnetic profiles are aligned at 32°W (long-dashed line), except for profiles A–A′ and B–B′, which are positioned such that the youngest anomalies are aligned with the equivalent anomalies on profile C–C′. The parts of profiles shown as white lines on a black background are interpreted as being affected by pseudofault crossings. ESR, East Scotia Ridge axis (dotted line); ARC, crest of island arc (dash–dot line); TRENCH, South Sandwich Trench axis (medium-dashed line). Short-dashed lines represent interpreted correlations between magnetic anomalies on observed and synthetic profiles. The synthetic profiles were calculated using the spreading rates shown, the geomagnetic polarity timescale of Cande & Kent (1995), the Definitive Geomagnetic Reference Field (DGRF) for 1985.0 (Barton 1996), the age–depth relationship for oceanic crust of Parsons & Sclater (1977), and a magnetic layer of 1 km thickness and susceptibility that decreases with increasing age (susceptibility (SI) 0.045 at 0 Ma, 0.024 at 0.68 Ma, 0.014 at 10 Ma, then constant for ages >10 Ma). Remanent magnetization vector inclinations, based on the assumptions that the time-averaged magnetic field approximates an axial geocentric dipole and there has been no significant change in latitude of the crust since its formation, were –72° for the northern synthetic profile and –73° for the southern one, with declination of 0° in both cases. The calculation of synthetic anomalies is based only on remanent magnetization, but the DGRF is used to calculate the component of the anomaly in the direction of the present magnetic field, as this is what observed total field anomalies measure. The reason that decreasing susceptibility with crustal age is used is to simulate the widely observed decay in anomaly amplitudes with increasing crustal age. The top of the magnetic layer in the model used to calculate the synthetic profiles was based on an oceanic age–depth relationship, rather than on observed bathymetric profiles, because the synthetic profiles are compared to a suite of observed magnetic profiles, and the bathymetry differs between profiles. Furthermore, using observed bathymetry would result in the top of the magnetic layer being too shallow wherever there is a significant thickness of sediment.

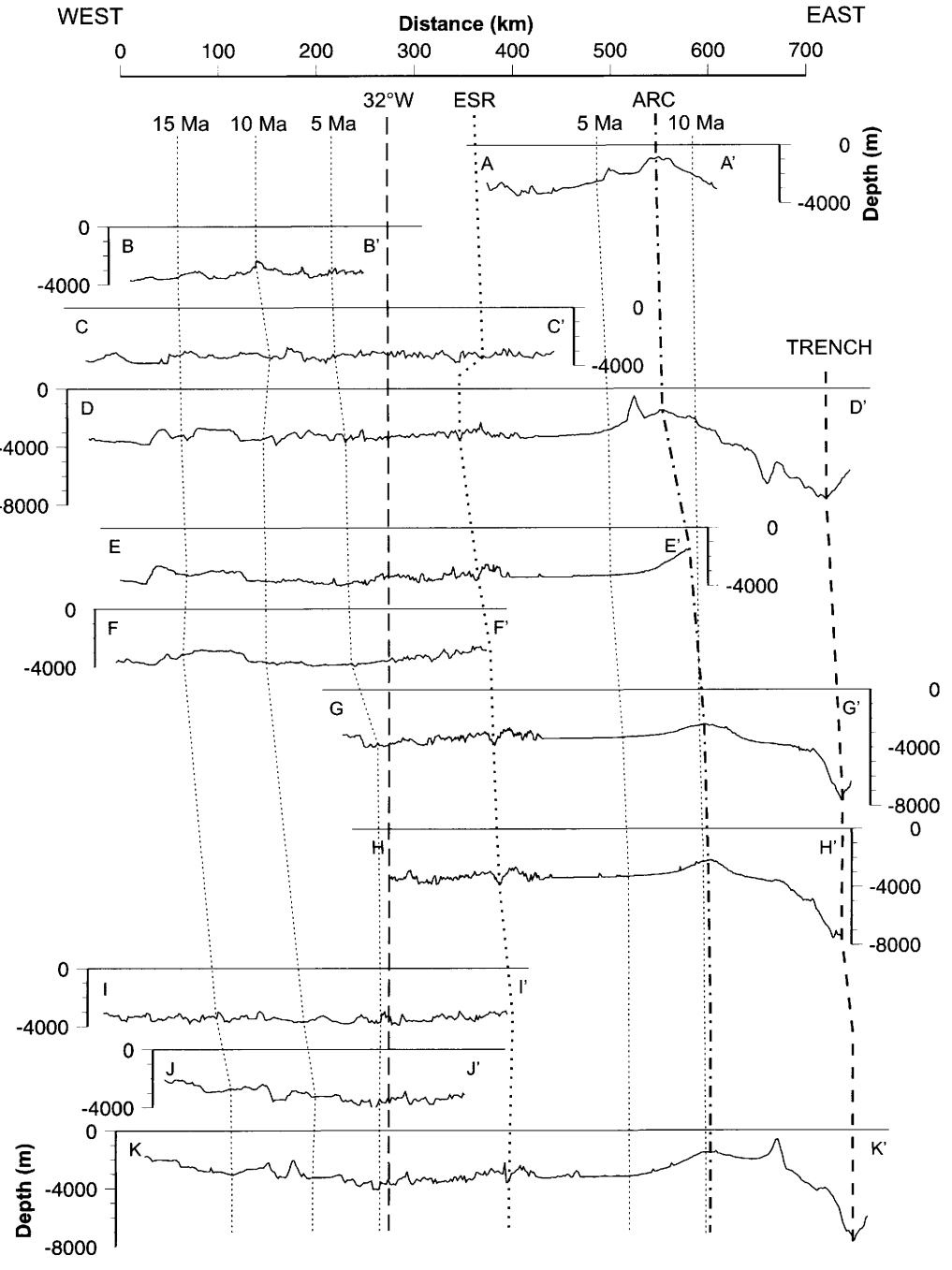


**Fig. 3.** East Scotia Sea bathymetry profiles along the same ship tracks as the magnetic profiles shown in Figure 2. Locations of profiles A–A′ to K–K′ are shown in Figure 1. All of the profiles are projected on to 090° . The profiles are aligned at 32°W, except for profiles A–A′ and B–B′, which are shown in the same relative positions as the coincident magnetic profiles in Figure 2. ESR, East Scotia Ridge axis (dotted line); ARC, crest of island arc (dash–dot line); TRENCH, South Sandwich Trench axis (medium-dashed line). Short-dashed lines represent lines of constant crustal age, based on interpretation of the coincident magnetic profiles, with ages annotated at the top of these lines.

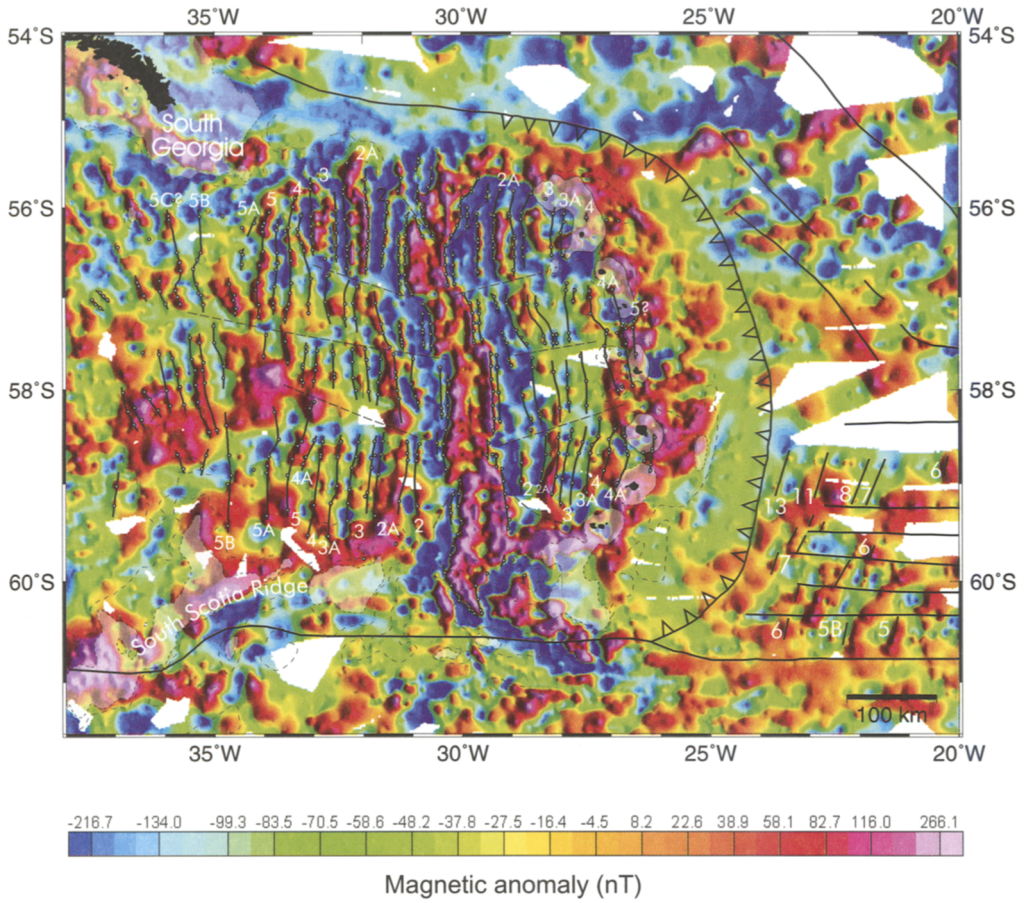


**Fig. 4.** Regional magnetic anomaly field, overlaid with the magnetic anomaly interpretation from Figure 1. The 2500 m (short-dashed lines) and 1500 m (pale, semi-transparent fill) bathymetric contours from Figure 1 are also shown. The regional field was calculated by subtracting the IGRF from all available marine magnetic profiles, carrying out cross-over error analysis on data from different cruises and sections of cruises, applying constant corrections to data from each cruise section and then gridding the corrected anomaly data. Interpolation was limited to 16 km from profiles, and areas further from the nearest profile appear white.

southern parts. Since the decrease in spreading rates 11.5 Ma ago, all subsequent spreading rates changes have been increases (Figs 2 and 5). Rates have increased in a series of steps on all parts of the ESR, eventually reaching the modern full rate of about 65 mm $a^{-1}$ 1.7 Ma ago. About 10 Ma ago half rates on the western flank of the ESR increased from 14 to 16 mm $a^{-1}$ in the north and from 12 to 14 mm $a^{-1}$ in the south. Spreading rates increased again 6 Ma ago, with western flank half rates increasing to 24 mm $a^{-1}$ in the north and 20 mm $a^{-1}$ in the south.

On the eastern flank of the ESR only magnetic anomalies younger than 10 Ma can be identified with confidence. Older back-arc crust must now lie beneath the inner forearc, but magnetic profiles across the forearc do not reveal consistent lineations, probably because the original magnetic record has been disturbed and overprinted as a result of arc magmatism (Vanneste & Larter 2002). Our tentative identifications of anomaly 5A (12.2 Ma) on profiles G–G′ and H–H′ imply that half rates between 12.2 and 10 Ma ago on the eastern flank of the ESR were about 13 mm $a^{-1}$ (Figs 2 and 5c). If these anomaly identifications are correct, spreading during this interval was approximately symmetrical. On the basis of more confidently identified anomalies, the reduced distance graphs indicate that spreading was approximately symmetrical between 10 and 6 Ma ago, with half rates on the eastern flank of

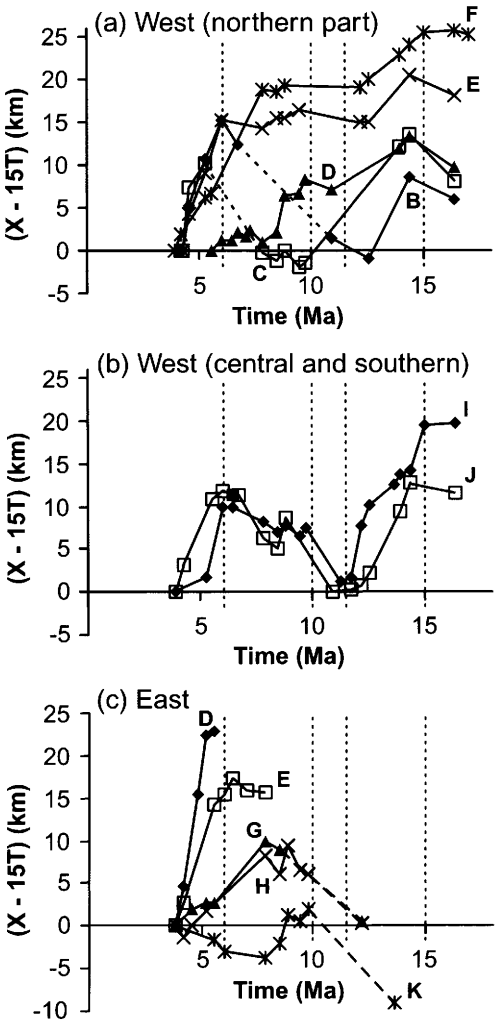


**Fig. 5.** Reduced distance graphs for the magnetic profiles shown in Figure 2, based on comparison with a synthetic profile generated using a constant half-spreading rate of 15 mm $a^{-1}$. Graph lines labelled B to K represent reduced distance data calculated from profiles B–B′ to K–K′, which are located in Figure 1. Vertical dotted lines indicate interpreted times of spreading rate changes. (**a**) Reduced distance graphs for profiles crossing the northern part of the west side of the East Scotia Sea. Short-dashed lines indicate probable pseudofault crossings. (**b**) Reduced distance graphs for profiles crossing the central and southern parts of the west side of the East Scotia Sea. (**c**) Reduced distance graphs for profiles crossing the east side of the East Scotia Sea. Long-dashed lines indicate parts of the graphs based on tentative identification of anomalies in the forearc.

the ESR averaging 16 mm $a^{-1}$. For the interval between 6 and 4 Ma ago, the fan-shaped pattern of graph lines in Figure 5c indicates substantial N–S variation in half spreading rates on the eastern flank of the ESR. During this interval eastern flank half rates ranged from about 25 mm $a^{-1}$ in the north to 14 mm $a^{-1}$ in the south. The systematic variation in spreading rates from north to south during this interval emerges as a result of our revised interpretation of anomalies in the NE part of the back-arc basin (see above). The earlier interpretation implied rates that increased from the southern to the central part of the ESR but were approximately constant along the central and northern part of the ESR, a pattern that is inconsistent with a rigid Sandwich Plate.

The most significant changes in spreading rate revealed by Figure 5 occurred 11.5 and 6 Ma ago. There was an overall reduction in spreading rates on the ESR 11.5 Ma ago, but the reduction was much greater in the south than in the north. About 6 Ma ago there was an overall increase in spreading rates, but the increase was much smaller in the south than in the north. Investigations of the South Scotia Ridge have revealed evidence for collisions between ancestors of the South Sandwich Trench and more westerly segments of the South American–Antarctic Ridge (Barker *et al.* 1984; Hamilton 1989). After each collision it appears that subduction stopped at the section of trench involved and rearrangement of plate boundaries transferred a sliver of back-arc lithosphere to the Antarctic Plate. However, the precise ages of collisions are poorly constrained. We suggest that such collisions are the most likely cause of the changes in spreading rates 11.5 and 6 Ma ago revealed by Figure 5. After each collision, spreading at the southern part of the ESR was probably slower than spreading at the northern part of the ridge while a new southern boundary to the Sandwich Plate became established (Fig. 6).

## Bathymetry profiles and age–depth relationships

Bathymetry data collected on the same ship tracks as the magnetic profiles shown in Figure 2 generally show a gradual increase in water depth with increasing distance from the ESR axis on its western flank (Fig. 3). On most of the profiles water depth increases from slightly less than 3000 m on the flanks of the axial troughs to between 3500 and 4000 m in the vicinity of anomaly 3A (5.9–6.6 Ma). This amount of subsidence is consistent with predictions of oceanic age–depth relationships (Trehu 1975; Parsons & Sclater 1977). However, farther west most profiles show seafloor depths becoming slightly shallower with increasing crustal age between

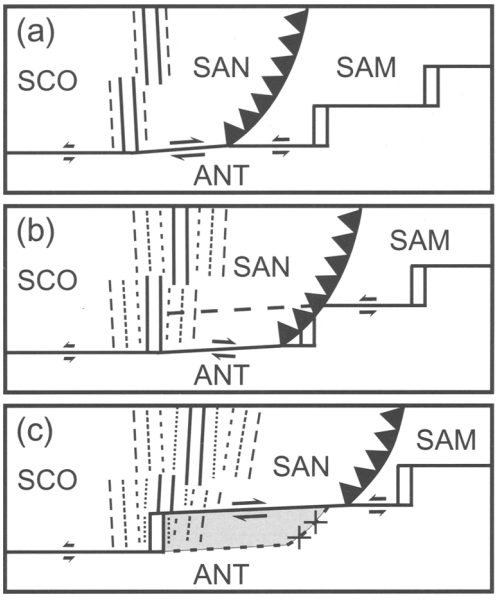


**Fig. 6.** Schematic illustrations showing postulated sequence of events resulting from collision of a South American–Antarctic Ridge segment with the southern end of the South Sandwich Trench. The positions of all features are shown relative to a fixed Antarctic Plate. (**a**) Pre-collision tectonic setting. Dashed lines represent magnetic anomalies recently formed at the East Scotia Ridge (SCO–SAN boundary). (**b**) Syncollision tectonic setting. Entry of young Antarctic Plate ocean floor into the southernmost part of the trench increases forces resisting subduction. This results in a N–S variation in spreading rates along the East Scotia Ridge, illustrated by short-dashed lines representing recently formed magnetic anomalies, and incipient rupture through the Sandwich Plate to form a new plate boundary north of the collision zone (long dashes). (**c**) Post-collision tectonic setting. Plate boundary north of the collision zone becomes established, resulting in transfer of a sliver of back-arc lithosphere to the Antarctic Plate (grey-shaded area), and creating a short spreading segment or transtensional zone on the South Scotia Ridge (SCO–ANT boundary). Spreading on East Scotia Ridge becomes uniform again, illustrated by dotted lines representing recently formed magnetic anomalies. Crosses represent the collision zone, where subduction has ceased.

anomalies 3A and 5r (6.6–11.5 Ma). In the vicinity of anomaly 5A (11.9–12.4 Ma) several profiles show a sharp decrease westwards in seafloor depths by more than 500 m, so the surface of some of the oldest crust in the East Scotia Sea lies at a similar depth to crust recently formed at the ESR. Seismic reflection profiles coincident with the western part of profiles E–E′ and F–F′ show that the sediment cover in that area is fairly uniform and has a thickness of 0.5 s two-way travel time (TWT) or less (<500 m), so the anomalous seafloor depths cannot be explained by thick sediment cover. Most of the back-arc basement on the eastern side of the ESR is buried beneath an arcward-thickening sediment apron (see the following section), so examination of age–depth relationships on that side of the back-arc basin would be a more complex exercise involving laterally variable correction for sediment loading.

Martinez & Taylor (2002) recently proposed a model for mantle wedge control on back-arc crustal accretion in which there are systematic variations in magma supply with distance from the arc volcanic front. The model predicts enhanced magma supply when a back-arc ridge is close to the arc volcanic front, on the basis that it is drawing on the arc mantle source, which is enriched in volatiles from the subducting slab. For a back-arc ridge located somewhat further from the arc volcanic front, the model predicts diminished magma supply, on the basis that melt at such a ridge is generated by advection of mantle that has been entrained above the subducting slab and has already been depleted by the extraction of arc magmas. This model provides a plausible explanation for the anomalous seafloor depths in the western part of the East Scotia Sea. During the formation of the oldest crust (before about 12 Ma) the back-arc ridge was probably close to the arc volcanic front, and enhanced magma supply would have produced anomalously thick back-arc crust, the surface of which would be shallower than predicted by standard oceanic age–depth relationships. As spreading continued the back-arc ridge migrated away from the arc volcanic front, and diminishing magma supply would have produced progressively thinner back-arc crust, resulting in the inverse age–depth relationship we observe today. The sharp change in seafloor depths observed on several profiles in the vicinity of anomaly 5A may indicate that there is an abrupt boundary within a broader transition region between the zones of 'enhanced' and 'diminished' magmatism.

## Seismic reflection profiles

MCS lines BAS967–34 and BAS967–36 (hereinafter referred to simply as 'line 34' and 'line 36', respectively) were acquired during RRS *James Clark Ross* cruise JR18 as part of the Sandwich Lithospheric and Crustal Experiment (SLICE; Larter *et al.* 1998). The locations of these lines are shown in Figure 1, and Figure 7 shows interpreted line drawings of the processed

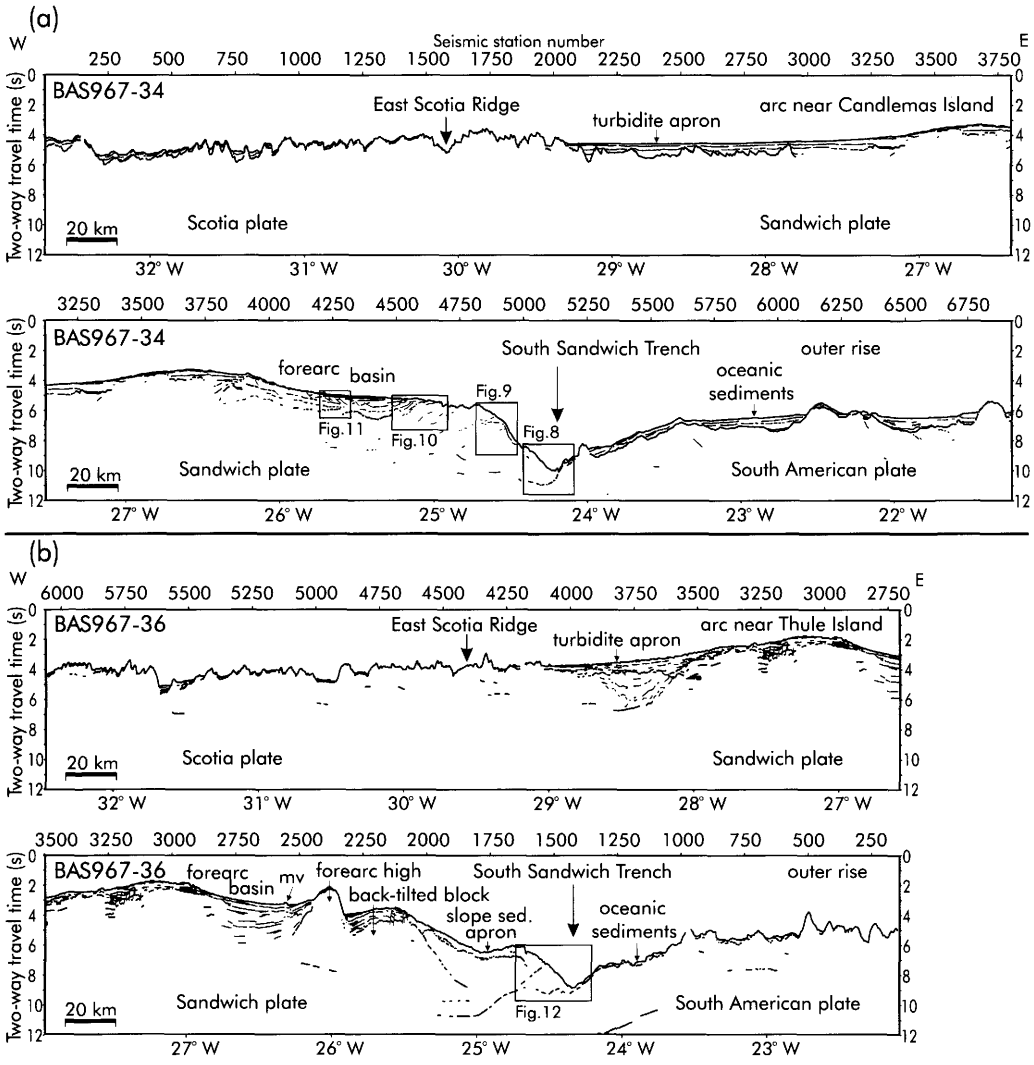


**Fig. 7.** Interpreted line drawings of multichannel seismic reflection profiles: (**a**) line BAS967-34; and (**b**) line BAS967-36. mv indicates mud volcano. Vertical exaggeration at the seafloor is 8: 1.

seismic profiles. The seismic source consisted of an array of 14 airguns with a total volume of 98 l (5976 in.$^3$). Shots were fired at a nominal spacing of 100 m to allow a sufficient interval between shots for simultaneous recording of wide-angle data on ocean-bottom seismometers (Larter *et al.* 2001). Ninety-six data channels were recorded at a 2 ms-sampling interval from a hydrophone streamer with an active length of 2400 m.

The standard processing sequence for both lines included resampling to 4 ms, bandpass filtering, predictive deconvolution, velocity analysis, stack (25 m common-depth point bins), Stolt $f$–$k$ migration (where $f$ is frequency and $k$ is wavenumber), time-variable bandpass filter, weighted trace mix and automatic gain control. The central part of line 34 was acquired in extremely adverse conditions that resulted in most of the hydrophone streamer towing at an undesirably shallow depth, introducing high levels of noise into the data. For the part of the line between the ESR and the trench, only data from the leading 12 channels of the streamer were processed, as these remained at an acceptable depth throughout this period. On line 36

additional processes were carried out on certain parts of the line. Before deconvolution, a weighted trace mix was applied to shot gathers between station numbers (SN) 1–1250 and 4175–6066 to attenuate coherent noise from the rough surface of oceanic basement. Before stacking the data, an *f–k* filter and inner-trace mute were applied to common-depth point gathers between SN 2018 and 4175 to suppress seafloor multiple reverberations.

Lines 34 and 36 both cross the entire South Sandwich subduction system, running from the outer rise in the east to the western flank of the back-arc basin. Line 34 crosses the northern part of the arc and is about 700 km long. It passes over the deepest saddle in the arc, which lies at a depth of 2400 m between Candlemas and Saunders islands (Fig. 1). Line 36 crosses the arc close to the southernmost group of islands, Southern Thule, and is about 600 km long (Fig. 1).

## *Line BAS967-34*

The eastern end of line 34 shows a variable thickness of sediment cover over the oceanic basement of the South American Plate on the outer rise (Fig. 7a), in the range 0–1 s TWT. On the basis of typical velocity–depth relationships for deep-water sediments (Hamilton 1979; Carlson *et al.* 1986) these travel times indicate a maximum sediment thickness of <1 km. The oceanic basement in this area has an age of about 55 Ma and was formed by NW–SE-directed spreading at the South American–Antarctic Ridge (Barker & Lawver 1988; Livermore & Woollett 1993). The basement highs between seismic station numbers (SN) 6100–6200 and 6800–6900 probably represent oblique crossings of ridges associated with small-offset fracture zones. When these highs are excluded, the average depth of the seafloor over the crest of the outer rise is 4700 m.

The trench axis on the line lies at a depth of 7600 m (Figs 7a and 8). Swath bathymetric data have shown that the axial depth of the trench is quite variable in this area, ranging from <7300 to >8100 m within 50 km either side of this line (Vanneste & Larter 2002).

The arc–trench gap measured along line 34 is 145 km (Fig. 7a). Among modern subduction zones only the New Hebrides, Solomon and New Britain systems have narrower arc–trench gaps (Jarrard 1986). The forearc can be divided into a broad inner forearc, with an average seafloor dip <1°, and a narrow outer forearc with an average seafloor dip >6° . Between these two areas there is an abrupt 'trench-slope break' at SN 4820, where the water depth is 4150 m (Figs 7a and 9).

Discontinuous reflections between 10 and 11 s TWT beneath the outer forearc probably represent the top of the subducted oceanic basement (Figs 7a and 8). A 'velocity pull-up' effect resulting from the dipping seafloor causes this surface to appear approximately horizontal on a travel time display, even though its true dip is to the west. Few other reflections are observed beneath the lower part of the outer forearc on this line, either on migrated or unmigrated data. Although data quality on the part of the line crossing the arc and forearc is compromised by the rough sea conditions that prevailed during acquisition, we do not think the scarcity of reflections beneath the outer forearc is caused by poor data quality. Subsurface features are clearly imaged beneath the upper part of the outer forearc and beneath the inner forearc (Figs 9 and 10) on data of similar quality, so if extensive coherent structures were present in the toe of the outer forearc slope we believe that they would be imaged.

A strong, horizontal reflection is observed beneath the upper part of the outer forearc slope at about 6.8 s TWT (Figs 7a and 9). The eastern end of this reflection terminates shortly before reaching the seafloor, at a point where the material beneath it is covered by a layer of slope sediment that is about 0.15 s TWT (<150 m) thick. However, the position where the projection of this reflection meets the seafloor coincides with an abrupt break in slope (at SN 4925). To the west of this point, the uppermost part of the outer forearc slope has a dip of 5°, while to the east a slope with a dip of 13° continues over a change in water depth of >800 m. This latter slope is much steeper than that on any modern accretionary prism (Lallemand *et al.* 1994) and lies within 20 km of the trench axis.

Analysis of the mechanics of accretionary prisms as critically tapered wedges suggests that such a steep surface slope could only be produced if the wedge material was unusually weak (had low 'effective internal friction'), the basal coupling was unusually strong or the basal décollement was at an unusually low angle (Davis *et al.* 1983). On the basis of this consideration, together with interpretation of gravity and four-channel seismic reflection data, Vanneste & Larter (2002) suggested that any frontal prism present along this part of the forearc is restricted to within a few kilometres of the trench.

In contrast, if the dominant process controlling evolution of the lower forearc in this area has been subduction erosion, as proposed by Vanneste & Larter (2002), the abrupt break of

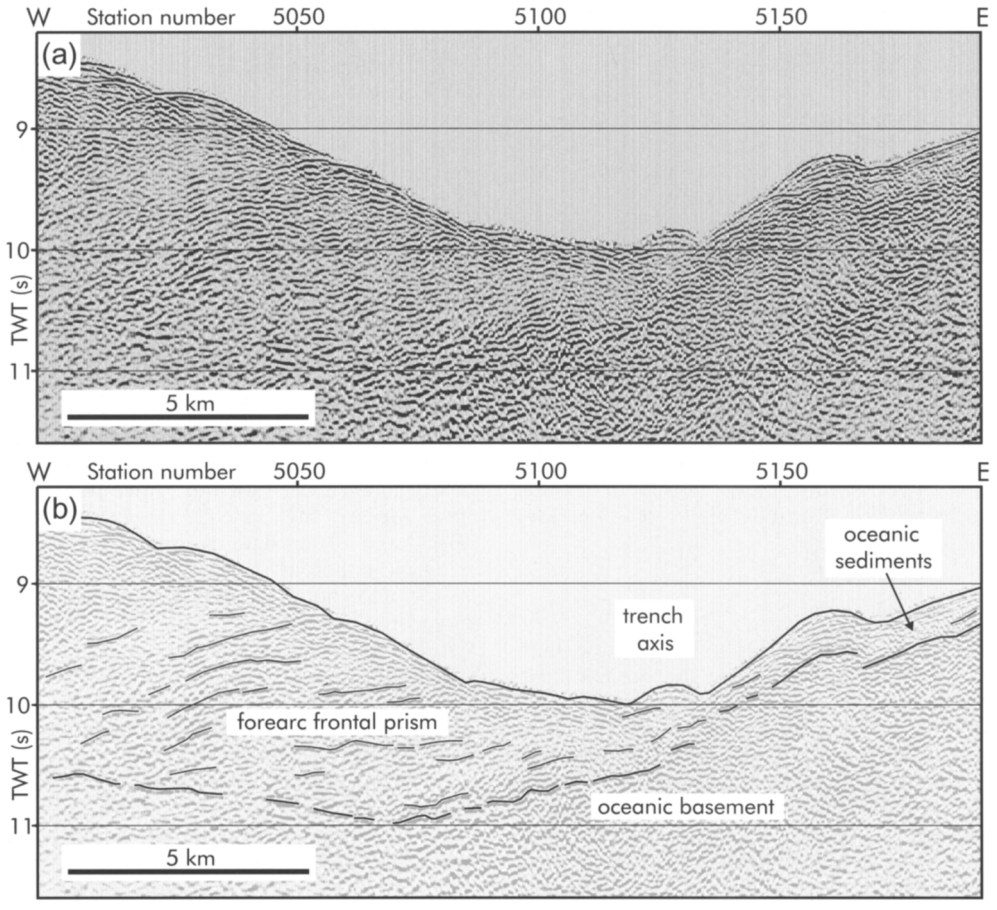


**Fig. 8.** Section of *f–k* migrated multichannel seismic line BAS967–34 crossing the trench and frontal prism. Vertical exaggeration at sea floor is 3.4: 1. Location of the section shown in Figure 7. TWT, two-way travel time. (**a**) Seismic data. (**b**) Interpretation of selected reflections overlaid on seismic data.

slope at SN 4925 suggests that the material beneath the reflector at 6.8 s TWT is significantly stronger than the overlying material. We speculate that this reflector is the top of the crustal basement on which the arc and forearc were built. Further detailed survey may reveal locations where the slope sediment cover is absent, allowing the supposed basement to be sampled by dredging.

A sedimentary basin extends across most of the inner forearc on line 34, with reflections being clearly imaged to depths of 1–1.5 s TWT (Figs 7a, 10 and 11). Velocity analyses on the MCS data, and wide-angle seismic data recorded on ocean-bottom seismometers, indicate that the average seismic interval velocity in the forearc basin sediments is about 2.5 km $s^{-1}$. Therefore, the thickness of sediments imaged on the MCS data in the central part of the basin varies between 1.2 and 1.9 km.

Forearc basin reflections at shallow depth near the eastern edge of the basin have a slight arcward dip and are truncated at the seafloor (Fig. 10). Deeper basin reflections in the same area dip more steeply and are truncated beneath an unconformity 0.17 s TWT below the seafloor. These reflection configurations indicate that the eastern part of the forearc basin has been subject to recent erosion, and there has been at least one previous episode of erosion during the development of the basin.

The MCS data show that the eastern edge of the forearc basin is affected by normal faults, most of which downthrow to the east and offset

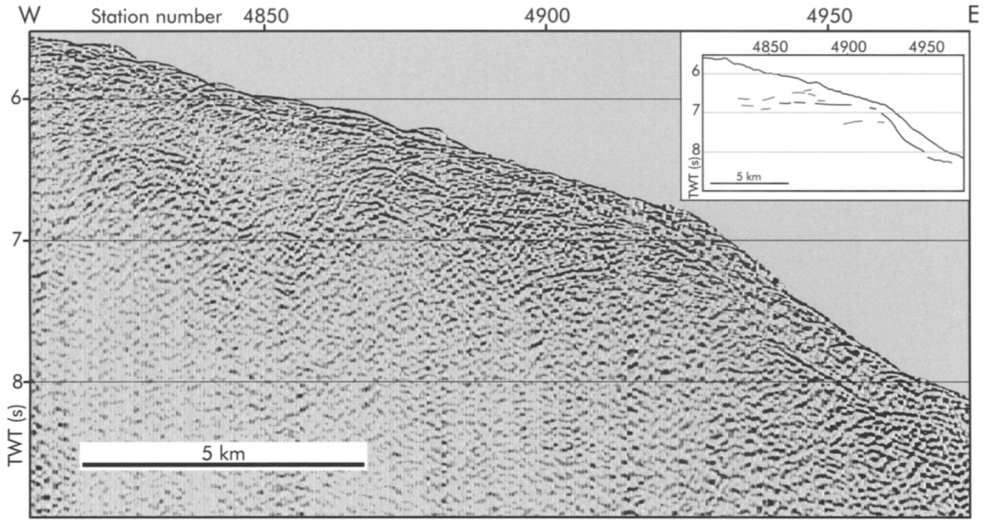


**Fig. 9.** Section of *f–k* migrated multichannel seismic line BAS967–34 crossing a break of slope on outer forearc. Location of the section shown in Figure 7. Inset shows interpreted reflections, including flat lying reflections at *c.* 6.8 s two-way travel time (TWT) that appear to be associated with the break in slope. Vertical exaggeration at the seafloor is 3.4: 1.

the seafloor (Fig. 10). Vanneste & Larter (2002) previously presented evidence for trench-parallel normal faults near the eastern edge of the basin in this area, based on side-scan sonar and four-channel seismic reflection data. Further west, however, the main part of the basin appears to be unaffected by such faulting. The only structural disruption affecting the main part of the basin is a set of low-angle extensional faults that sole out within the basin sediments (Fig. 11).

The MCS data do not reveal a distinct western boundary to the forearc basin. Reflections at shallow depth appear to continue across the saddle in the arc between Candlemas and Saunders islands, while deeper basin reflections become progressively less continuous westward and eventually disappear into a unit with chaotic seismic facies beneath the arc crest (Fig. 7a).

A sedimentary apron up to 1 s TWT thick (up to *c.* 1 km) extends to about 160 km west of the arc crest on line 34 and covers most of the back-arc basement east of the ESR (Fig. 7a). Reflections within the sediment apron are subhorizontal and very continuous, suggesting that it consists mostly of arc-derived turbidites.

Line 34 crosses the middle of segment E5 of the ESR about 210 km west of the arc crest. At this point segment E5 exhibits a median valley approximately 8 km wide with 600–750 m relief. No subseafloor reflections have been identified beneath the axial valley, but the seafloor profile across its eastern flank suggests the presence of a 'staircase' of normal faults with about 3 km spacing and downthrows to the west (Fig. 7a). Further away from the ridge both its flanks exhibit asymmetric basement topography, with parts of the basement surface that dip towards the ridge generally having steeper gradients than parts that dip away from the ridge. We interpret this observation as evidence that the spreading process involved rotational block faulting.

To the west of the ESR sediment thickness generally increases with increasing distance from the ridge, and hence with increasing crustal age. The sediment thickness reaches about 0.6 s TWT (<600 m) near the western end of the line, where the oceanic basement age is 6 Ma (Fig. 1). The basement ridge at SN 100–200 coincides with an oblique crossing of a pseudofault (Figs 1 and 2).

## *Line BAS967-36*

A *f–k* migrated profile showing data from the entire length of line 36 has been published previously (Vanneste *et al.* 2002). Below we describe the main differences between this line and line 34.

The oceanic basement presently entering the trench where line 36 crosses it has an age of about 27 Ma. Although fracture zones to the east

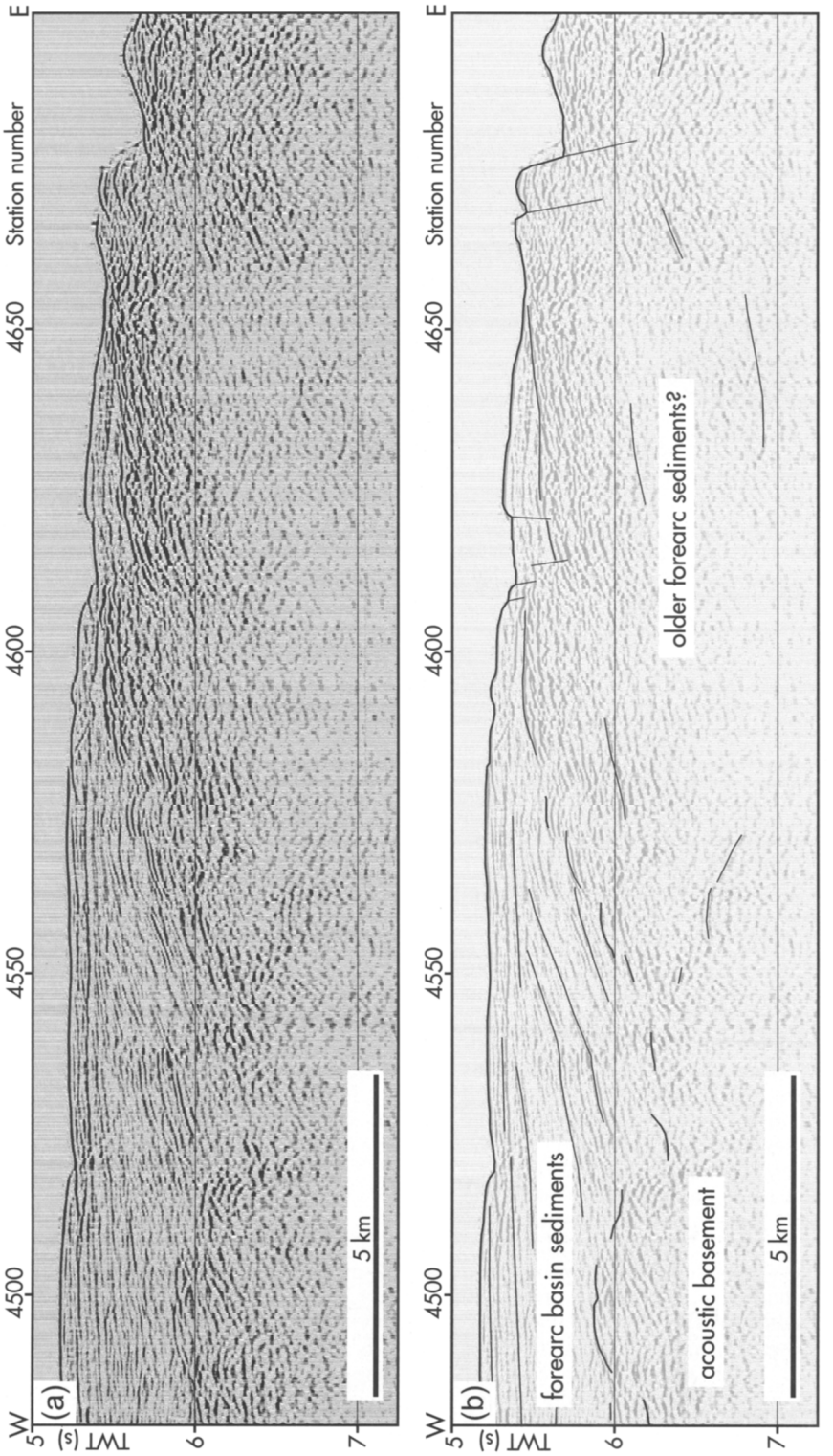


**Fig. 10.** Section of *f–k* migrated multichannel seismic line BAS967-34 crossing the eastern edge of the inner forearc basin. Vertical exaggeration at seafloor is 3.4:1. Location of the section shown in Figure 7. TWT, two-way travel time. (**a**) Seismic data. (**b**) Interpretation of selected reflections overlaid on seismic data.

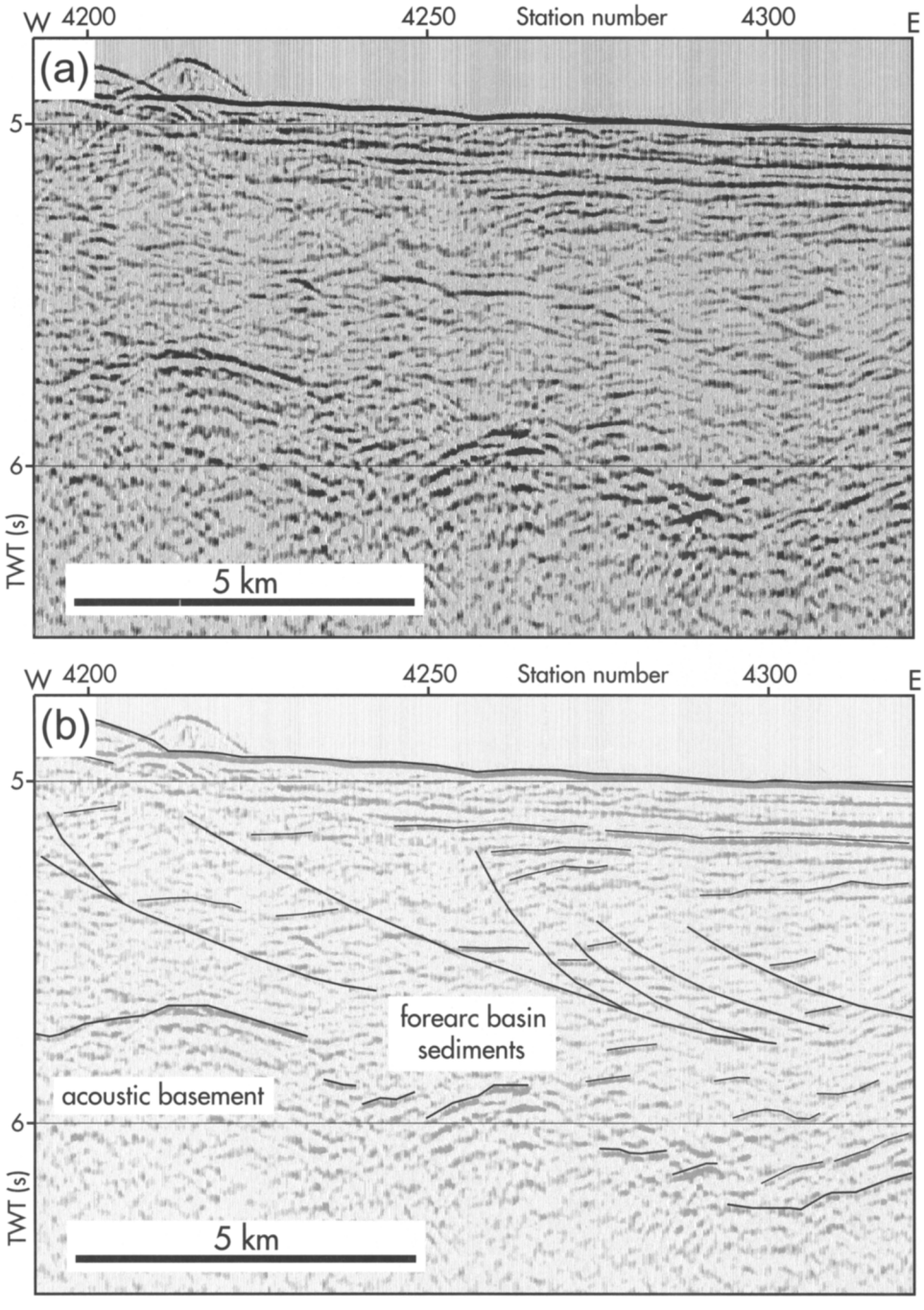


**Fig. 11.** Section of *f–k* migrated multichannel seismic line BAS967–34 crossing the central part of the inner forearc basin, showing low-angle extensional faulting within the forearc basin sediments. Vertical exaggeration at the seafloor is 6.8: 1. Location of the section shown in Figure 7. TWT, two-way travel time. (**a**) Seismic data. (**b**) Interpretation of selected reflections overlaid on seismic data. The mound that is observed centred about SN 4215 is interpreted as being out of the plane of the section.

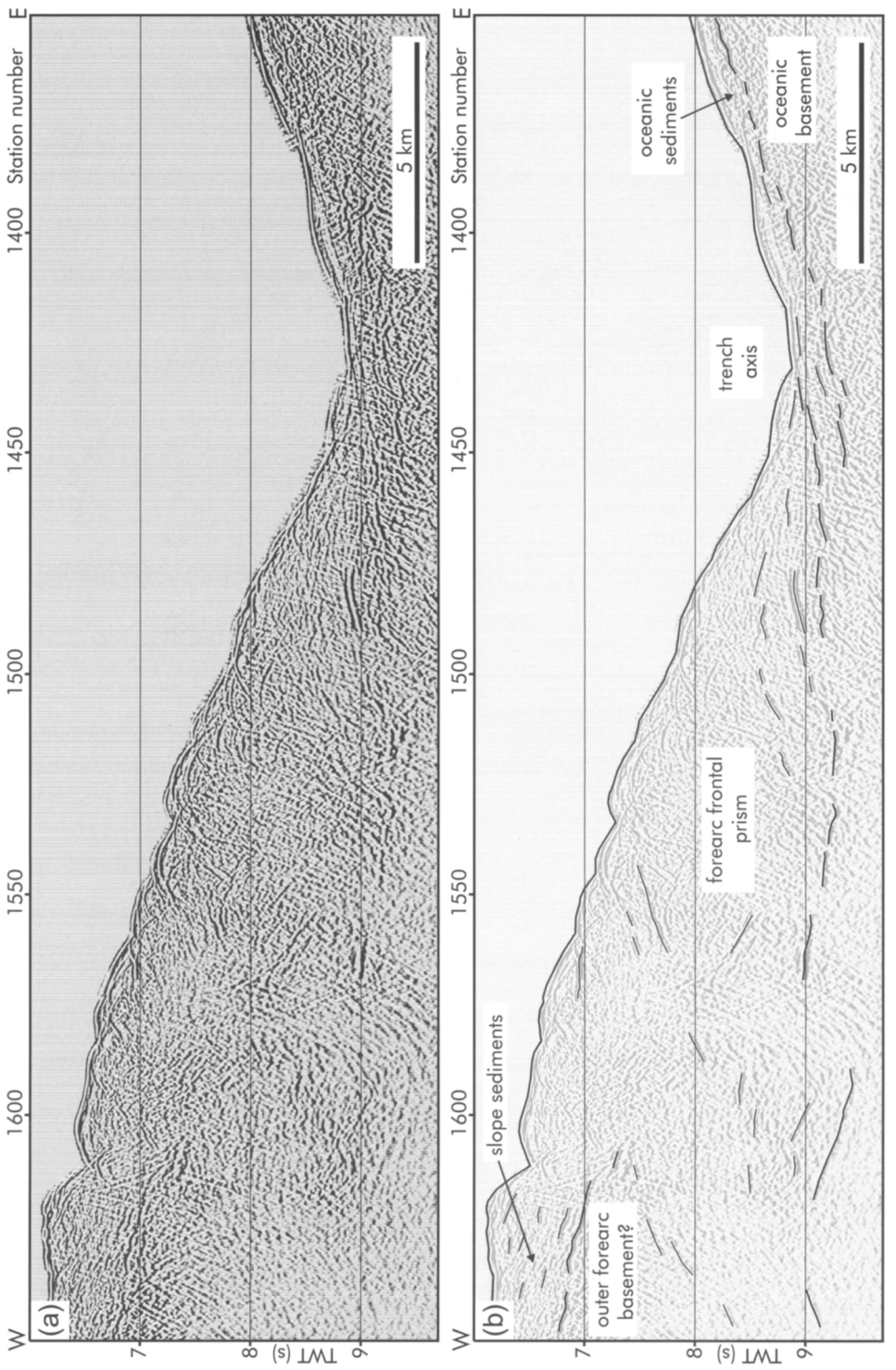


**Fig. 12.** Section of *f–k* migrated multichannel seismic line BAS967–36 crossing the trench and frontal prism. Vertical exaggeration at the seafloor is 3.4:1. Location of the section shown in Figure 7. TWT, two-way travel time. (**a**) Seismic data. (**b**) Interpretation of selected reflections overlaid on seismic data.

of the southern part of the trench trend E–W (Fig. 1), they have formed since a change in the direction of South American–Antarctic relative motion at about 20 Ma (Barker & Lawver 1988). Prior to this the spreading direction at the South American–Antarctic Ridge was NW–SE, and all of the South American ocean floor consumed at the South Sandwich Trench thus far was formed by spreading with this earlier orientation.

The sediment cover overlying oceanic basement on the outer rise on line 36 is 0–0.2 s TWT thick (<200 m), which is much less than the average thickness of the cover on the older basement on line 34. The average seafloor depth over the crest of the outer rise (3900 m) is also much shallower on line 36, as is the depth of the trench axis, at 6680 m (Figs 7b and 12).

The arc–trench gap measured along line 36 is 160 km (Fig. 7b), which is slightly greater than on line 34. However, the biggest difference between the two lines is in the topography and structure of the forearc.

On line 36 a forearc high separates a narrow inner forearc from a broad outer forearc (Fig. 7b). The outer forearc slope has a stepped appearance, as it includes two gently arcward-dipping terraces. Across most of the outer forearc slope, a sediment apron that is 0.2–0.7 s TWT thick (*c.* 200–700 m) and has a chaotic seismic facies overlies a band of strong reflections. This band of reflections ends abruptly at SN 1610, 18 km west of the trench (Fig. 12). Between this point and the trench axis is the steepest part of the outer forearc slope, with an average seafloor dip of 6.6°. This part of the slope is the surface of a frontal prism that has a thickness of up to 2.5 s TWT (>2.5 km). The base of the frontal prism is constrained by a strong and fairly continuous reflection that can be traced for nearly 50 km from the trench beneath the outer forearc and has been interpreted as the top of subducted oceanic basement (Vanneste *et al.* 2002).

The frontal prism on line 36 has a chaotic seismic facies similar to that of the slope sediment apron, but distinct from the almost reflection-free material beneath the slope apron to the west (Fig. 12). The frontal prism appears to taper arcward beneath the material to its west. Only one extensive reflection is clearly imaged within the prism, dipping arcward from just below the seafloor at SN 1530 (Fig. 12). We interpret this reflection as a thrust fault. As on line 34, we interpret the scarcity of reflections beneath the toe of the outer forearc slope as indicating that extensive coherent structures, such as those imaged in frontal prisms where active sediment accretion is taking place (Westbrook *et al.* 1988; Moore *et al.* 1990; Bangs *et al.* 1996; Park *et al.* 2002), are rare here.

The eastern flank of the forearc high on line 36 is a 1200 m-high escarpment that exposes reflection-free forearc basement and stands above a 20 km-wide arcward-dipping terrace. The MCS data show that stratified sediments up to 1.3 s TWT thick (>1 km) lie beneath the terrace, and within these sediments there are upward transitions in reflection configurations from parallel with the top of basement, to arcward divergent, to parallel and horizontal (Fig. 7b). These reflection configurations indicate rotation of a 20 km-wide fault block underlying the terrace. The seismic data also reveal small normal faults that offset the seafloor near the trenchward edge of the terrace. To the east of the terrace, breaks in slope of the seafloor (at SN 2040) and of the base of the slope sediment apron (at SN 2020) coincide with the upward projection of a 20 km-long, trenchward-dipping, weak and discontinuous reflection (Fig. 7b), which we interpret as a low-angle detachment fault.

A sedimentary basin extends across most of the inner forearc on line 36, as on line 34 (Fig. 7). Once again, only the eastern edge of the basin appears to have been subject to structural disturbance, and a 100 m-high mound that has been interpreted as a mud volcano is situated above the westernmost fault (Vanneste *et al.* 2002). Shallow earthquake hypocentres (Engdahl *et al.* 1998) and focal mechanisms are consistent with the interpretation that the western limit of active faulting is near the eastern edge of the forearc basin (Vanneste *et al.* 2002).

The forearc basin on line 36 differs from the one on line 34 in that its maximum thickness is considerably greater and the seismic data do not suggest that any part of the basin has been subject to recent erosion. Velocity analyses on the MCS data, and wide-angle seismic data recorded on ocean-bottom seismometers, indicate that seismic interval velocities in the forearc basin sediments on line 36 increase from <2.0 km $s^{-1}$ near the seafloor to >2.5 km $s^{-1}$ at 1 km below seafloor (bsf) and to >4.0 km $s^{-1}$ at 3 km bsf. The velocity data imply that the deepest clearly imaged reflection in the basin, at 2.85 s TWT bsf, is at a depth of >4 km bsf.

As on line 34, the MCS data on line 36 do not reveal a distinct western boundary to the forearc basin. Reflections become progressively less continuous westward until they disappear into a unit with chaotic seismic facies beneath the arc near Southern Thule. Another similarity is the presence of a sedimentary apron that is up to 1 s TWT thick (up to *c.* 1 km) on the western flank

of the arc, although on line 36 it only extends to about 105 km west of the arc crest (Fig. 7b).

Line 36 crosses the middle of segment E8 of the ESR about 140 km west of the arc crest (Fig. 7b). Swath bathymetric data have shown that along most of its 90 km length, ridge segment E8 exhibits a median valley approximately 12 km wide with 300–800 m relief (Bruguier & Livermore 2001). However, a topographic high, offset towards the eastern wall, occurs within the valley where line 36 crosses it (SN 4350–4480).

The volcanic basement to the west of the ESR on line 36 exhibits a similar asymmetric topography to that observed on line 34, with parts of the basement surface that dip towards the ridge generally having steeper gradients than parts that dip away from the ridge (Fig. 7b). Sediment cover to the west of the ESR on line 36 is generally thinner and more unevenly distributed than on line 34. The thickest sediment cover on this part of line 36 is in the deepest trough (SN 5580–5610), and is about 0.5 s TWT (<500 m). However, the average sediment thickness between this trough and the western end of the line, over basement that ranges in age between 3.3 and 5.3 Ma, is <0.2 s TWT (<200 m).

## Gravity modelling

Gravity data were collected on cruise JR18 using a LaCoste and Romberg marine gravity meter. Base ties at Port Stanley, Falkland Islands at the start and end of the 55 day-long cruise indicated an overall meter drift of only +0.13 mGal.

The gravity data collected along MCS lines 34 and 36 were modelled to constrain crustal thickness variations across the arc and forearc, and to estimate the density of the outer forearc crust. The objectives of modelling were not to determine precise or detailed crustal cross-sections, but to examine what constraints gravity data place on crustal thickness and outer forearc density. Two-dimensional gravity models were constructed for each line, starting with the bathymetry data that were collected along the MCS lines.

In any marine gravity model the largest contribution to local free-air gravity anomaly variations is from seafloor topography, which commonly represents a density contrast of >1 Mg $m^{-3}$ (i.e. $10^6$ g $m^{-3}$). Unless there are large variations in sediment thickness, the second largest contribution is usually from the base of the crust (the Moho), which typically represents a density contrast of approximately 0.4 Mg $m^{-3}$. Therefore, simple gravity models comprising only sea water, crust and mantle can provide a quick estimate of crustal thickness variations, assuming that no other significant density contrasts are present.

Jull & Kelemen (2001) recently calculated that some arc lower crust lithologies have densities similar to, or greater than, the underlying mantle at pressures >0.8 GPa and temperatures <800°C. Therefore, gravity models may be insensitive to arc lower crust at depths where the pressure is >0.8 GPa. However, for crust consisting mainly of basaltic and gabbroic lithologies, 0.8 GPa is equivalent to a depth of about 28 km. Our gravity modelling results indicate a maximum crustal thickness that is significantly less than this threshold, so it is unlikely that such ultra-high-density lower crust is present beneath the South Sandwich arc.

To obtain absolute crustal thickness estimates from simple gravity models of the kind described above it is necessary for the thickness of the crust to be known or assumed at one point within the model. In the models presented here (Figs 13 and 14) the initial assumption was that the crust on the South American Plate is normal oceanic crust with a thickness of 7 km. On the

**Fig. 13.** Gravity models for multichannel seismic line BAS967–34. For each model the calculated free-air anomaly profile is shown as a dashed line and the observed profile is shown as a solid line. The apparent thinning of subducted crust with increasing slab dip is an artefact of the 4.3: 1 vertical exaggeration. (**a**) Model assuming a uniform crustal density, a uniform mantle density, and that crust to the east of the trench and subducted crust have a constant thickness of 7 km. (**b**) Model assuming a uniform crustal density, and that crust to the east of the trench, subducted crust and back-arc crust all have a constant thickness of 7 km, but allowing different mantle densities either side of the subducted crust. (**c**) Model modified from that in (**b**) by the introduction of sediment bodies observed on a multichannel seismic line, adjustment of arc Moho to compensate for effect of sediments, and the introduction of additional intermediate-density bodies required to match the calculated anomaly to the observed anomaly over the outer forearc and trench. Inset shows detail of the outer forearc and trench part of model. (**d**) Model modified from that in (**c**) by extension of the base of model to 150 km depth, introduction of an eclogite layer in place of subducted crust below 60 km and adjustment of the mantle density beneath the back-arc and arc. Then Moho beneath arc and forearc was adjusted to compensate for other changes. Models in (**a**)–(**c**) continue 200 km to either end of the observed anomaly profile to minimize edge effects on the calculated profile. Model (**d**) continues 400 km to either end of the observed profile.

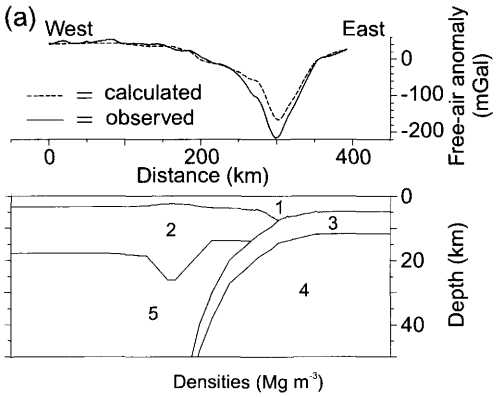


Densities (Mg m$^{-3}$)

1 = 1.03 water
2 = 2.89 arc crust
3 = 2.89 oceanic crust
4 = 3.30 oceanic mantle
5 = 3.30 sub-arc mantle

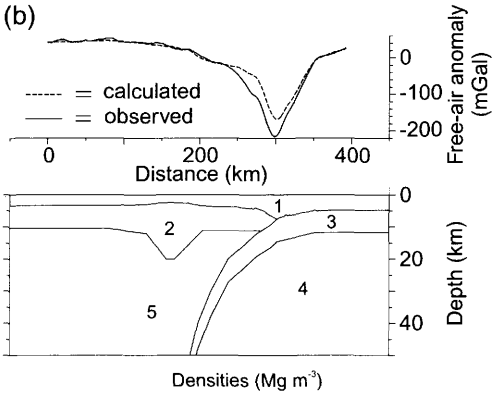


Densities (Mg m$^{-3}$)

1 = 1.03 water
2 = 2.89 arc crust
3 = 2.89 oceanic crust
4 = 3.30 oceanic mantle
5 = 3.22 sub-arc mantle

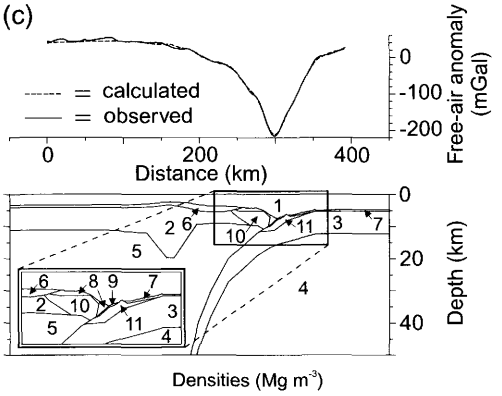


Densities (Mg m$^{-3}$)

1 = 1.03 water
2 = 2.89 arc crust
3 = 2.89 oceanic crust
4 = 3.30 oceanic mantle
5 = 3.225 sub-arc mantle
6 = 2.20 arc-forearc sediment
7 = 2.20 outer rise sediment
8 = 2.20 outer forearc sed.
9 = 2.20 trench sediment
10 = 2.50 outer forearc crust
11 = 2.50 alt. oceanic crust

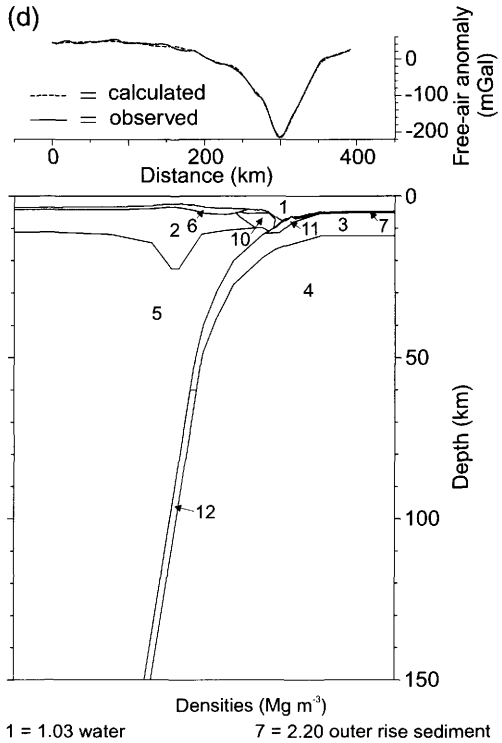


Densities (Mg m$^{-3}$)

1 = 1.03 water
2 = 2.89 arc crust
3 = 2.89 oceanic crust
4 = 3.30 oceanic mantle
5 = 3.275 sub-arc mantle
6 = 2.20 arc-forearc sed.
7 = 2.20 outer rise sediment
8 = 2.20 outer forearc sed.
9 = 2.20 trench sediment
10 = 2.50 outer forearc crust
11 = 2.50 alt. oceanic crust
12 = 3.55 eclogite

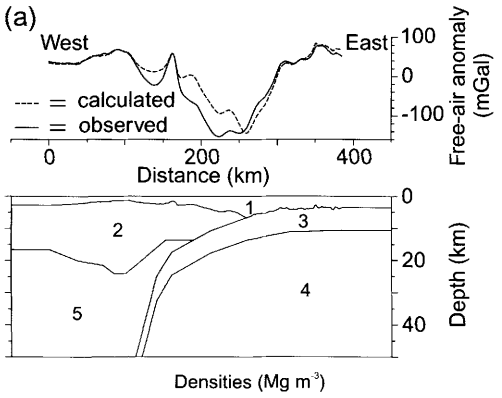


1 = 1.03 water
2 = 2.89 arc crust
3 = 2.89 oceanic crust
4 = 3.30 oceanic mantle
5 = 3.30 sub-arc mantle

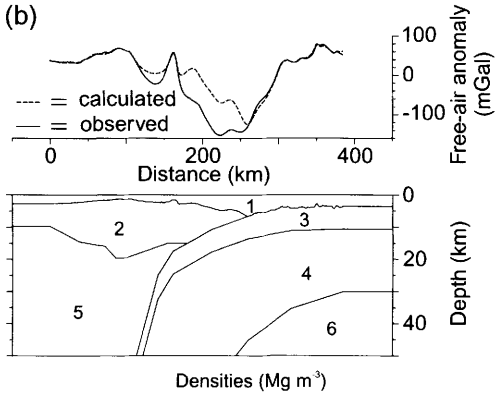


1 = 1.03 water
2 = 2.89 arc crust
3 = 2.89 oceanic crust
4 = 3.30 oceanic mantle 1
5 = 3.197 sub-arc mantle
6 = 3.22 oceanic mantle 2

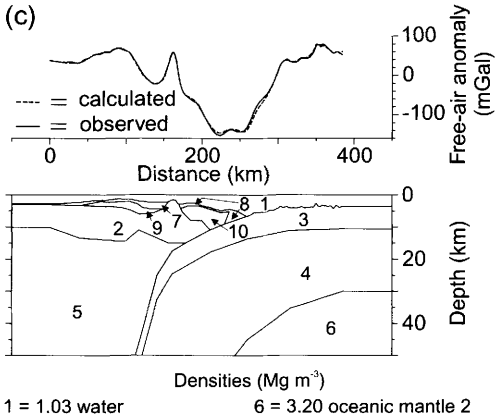


1 = 1.03 water
2 = 2.89 arc crust
3 = 2.89 oceanic crust
4 = 3.30 oceanic mantle 1
5 = 3.195 sub-arc mantle
6 = 3.20 oceanic mantle 2
7 = 2.20 arc-forearc sed. 1
8 = 2.20 outer forearc sed.
9 = 2.50 arc-forearc sed. 2
10 = 2.45 outerf orearc crust

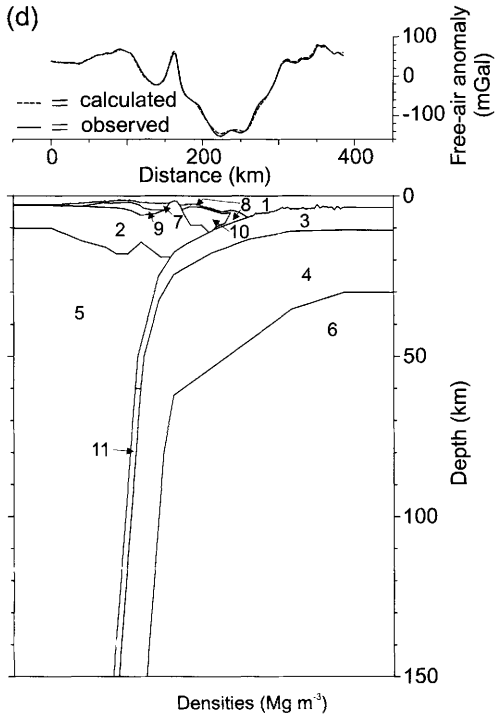


1 = 1.03 water
2 = 2.89 arc crust
3 = 2.89 oceanic crust
4 = 3.35 oceanic mantle 1
5 = 3.244 sub-arc mantle
6 = 3.25 oceanic mantle2
7 = 2.20 arc-forearc sed.1
8 = 2.15 outerforearc sed.
9 = 2.50 arc-forearc sed.2
10 = 2.43 outer forearc crust
11 = 3.55 eclogite

basis of a compilation of seismic refraction results, White *et al.* (1992) concluded that the igneous section of oceanic crust averages 7.1±0.8 km thick away from anomalous regions such as fracture zones and hot spots. Regional bathymetry data from the South American Plate to the east of the outer rise are generally in close agreement with depths predicted from oceanic age–depth relationships (Barker & Lawver 1988), suggesting that the crust in this area is of normal thickness.

On both lines 34 and 36 it was found that simple models of the type described above imply unrealistically thick back-arc crust, and cannot explain the full magnitude of the negative anomaly over the outer forearc and trench (Figs 13a and 14a). The models were extended 200 km from both ends of the modelled gravity profile to minimize edge effects. The position of the subducted oceanic crust was based on consideration of earthquake hypocentre locations (Engdahl *et al.* 1998; Vanneste *et al.* 2002; Livermore 2003). All of the crust in these models was assigned a density of 2.89 Mg $m^{-3}$, the average density of igneous oceanic crust estimated by Carlson & Raskin (1984). The average density of the arc crust and forearc crust is probably slightly lower than that of oceanic crust due to the presence of a larger proportion of lithologies with higher Si contents, and thick volcanic and volcaniclastic units. However, using lower densities for the arc and forearc crust would result in the modelled crust being thinner in these areas. Therefore, models including oceanic crustal density are used to examine the constraints gravity data place on maximum thickness of the crust. The mantle in the initial models was assigned a uniform density of 3.3 Mg $m^{-3}$, which approximates the average density of abyssal peridotite above 100 km-depth for an intermediate geothermal gradient (Christensen & Mooney 1995; Jull & Kelemen 2001).

On both lines the western limit of the modelled gravity data is over crust that formed at the ESR since 2 Ma. Line 36 crosses segment E8 of the ESR about 140 km west of the arc. A lone earthquake hypocentre at a depth of 273 km and located 20 km east of segment E8 (Engdahl *et al.* 1998) provides the only clue to the depth of the slab beneath this part of the ESR. At this distance from the volcanic front and this elevation above the slab, subduction-related processes probably have only a minor influence on magma supply to back-arc spreading ridges (Martinez & Taylor 2002, 2003). Line 34 crosses segment E5 of the ESR about 210 km west of the arc crest, and earthquake hypocentres suggest that the top of the slab has already reached a depth of 300 km more than 100 km to the east. Therefore, we consider it unlikely that subduction influence would have caused the crust produced recently at either of these segments to be thicker than normal oceanic crust.

Swath bathymetry data (Bruguier & Livermore 2001; Livermore 2003) show that the average depth over the flanks of the axial troughs on segments E5 and E8 is about 2.8 km. This is slightly deeper than the 2.5 km average for the world's mid-ocean ridges calculated by Parsons & Sclater (1977) and suggests that the young back-arc crust may, in fact, be slightly thinner than normal oceanic crust.

As it seems unlikely that the back-arc crust is thicker than normal oceanic crust, another pair of gravity models was produced in which the additional assumption was made that the back-arc crust is 7 km thick (Figs 13b and 14b). The observed regional anomaly trend was then matched by reducing the density of the mantle body beneath the back-arc and arc. In a similar

**Fig. 14.** Gravity models for multichannel seismic line BAS967–36. For each model the calculated free-air anomaly profile is shown as a dashed line and the observed profile is shown as a solid line. The apparent thinning of subducted crust with increasing slab dip is an artefact of the 4.3: 1 vertical exaggeration. (**a**) Model assuming a uniform crustal density, a uniform mantle density, and that crust to the east of the trench and subducted crust have a constant thickness of 7 km. (**b**) Model assuming a uniform crustal density, and that crust to the east of the trench, subducted crust and back-arc crust all have a constant thickness of 7 km, but allowing different mantle densities either side of the subducted crust. The mantle on the eastern side of the model is divided into two bodies to simulate the lateral density variation in young oceanic lithosphere that is the probable cause of the different calculated and observed anomaly gradients observed on this part of the model in (**a**). (**c**) Model modified from that in (**b**) by the introduction of sediment bodies observed on multichannel seismic line, adjustment of arc Moho to compensate for effect of sediments, and the introduction of additional intermediate-density bodies required to match the calculated anomaly to the observed anomaly over the outer forearc and trench. (**d**) Model modified from that in (**c**) by extension of the base of the model to 150 km depth, introduction of eclogite layer in place of subducted crust below 60 km and adjustment of mantle densities. Then the outer forearc structure and Moho beneath the arc were adjusted to compensate for other changes. Models in (**a**)–(**c**) continue 200 km to either end of the observed anomaly profile to minimize edge effects on the calculated profile. Model (**d**) continues 400 km to either end of the observed profile.

gravity modelling exercise on a profile across the Mariana arc, Sager (1980) also found that it was necessary to include a low-density mantle body beneath the back-arc in order to allow the overlying crust to have a normal thickness. Furthermore, Sager (1980) calculated that the required density anomaly depended on the depth chosen as the base of the anomalous mantle body, decreasing from –0.057 Mg $m^{-3}$ for a body with its base at 100 km depth to –0.033 Mg $m^{-3}$ for a body with its base at 200 km depth.

The base of most of the models presented here was fixed at a depth of 50 km, and it was found that mantle density anomalies of –0.078 (line 34) and –0.083 Mg $m^{-3}$ (line 36) were required to match the regional anomaly trend. We recognize that these density anomalies are unrealistically high and have used them as a crude way of approximating a mass deficiency that probably extends to greater depth. The lower density contrast at the Moho beneath the arc results in the arc crust in the model being slightly thicker than it would be if a more normal mantle density was used and the regional anomaly trend was matched by adjusting the model in a different way (e.g. extending it to greater depth or increasing the density of the South American Plate mantle).

A model for line 34 extended to 150 km depth (Fig. 13d) requires a back-arc and arc mantle with a density anomaly of –0.025 Mg $m^{-3}$, which seems more realistic and is equivalent to an average temperature anomaly of about +300°C relative to the South American Plate mantle (using a volumetric coefficient of thermal expansion for peridotite of $2.4 \times 10^{-5}$ $K^{-1}$). The back-arc and arc mantle density anomaly in a model for line 36 extended to 150 km depth (Fig. 14d) cannot be described so simply, as it was found to be necessary to divide the South American mantle into two bodies to simulate lateral density variation in the young oceanic lithosphere approaching the trench in this area. The extension of the models to greater depth required only minor changes to the crustal profile across the arc, so we consider that this justifies our approach of limiting initial models to a depth of 50 km for preliminary estimation of crustal thickness variations. The deeper models were also extended an additional 200 km from both ends of the modelled gravity profile to minimize edge effects (i.e. 400 km from each end in total). The changes to the crustal profiles after extending the models to 150 km depth were mainly due to the inclusion of an eclogite layer at the top of the subducted slab rather than to the depth extension itself.

The simple gravity models considered thus far do not take account of the effect of sediment bodies. Insertion of a sediment body into these models introduces a mass deficit that requires adjustment of the underlying Moho to shallower depth to maintain the same calculated anomaly. Therefore, the models without sediments (Figs 13b and 14b) constrain the maximum possible crustal thickness, subject to the assumptions described above.

A third pair of gravity models was produced including sediment bodies observed on the MCS lines (Figs 13c and 14c). Our aim was still to use these models to constrain the maximum possible crustal thickness beneath the arc and forearc, and for this reason sediment bodies extending to a depth of <2 km below seafloor were all assigned the relatively high density of 2.2 Mg $m^{-3}$. This density is equivalent to a seismic velocity of 2.5–3.0 km $s^{-1}$ according to the velocity–density relationships of Ludwig *et al.* (1970) and Gardner *et al.* (1974), which is quite a high average velocity for the upper 2 km of deep ocean sedimentary successions (Hamilton 1979; Carlson *et al.* 1986). More deeply buried inner forearc basin sediments on line 36 were assigned a density of 2.5 Mg $m^{-3}$, which is equivalent to a seismic velocity of 4.3–4.8 km $s^{-1}$ according to the above relationships. We also used this pair of models to investigate what average density of outer forearc crust was required to account for the large negative anomaly over the outer forearc on each line (Figs 13c and 14c).

Travel-time inversion of wide-angle seismic data recorded on ocean-bottom seismometers will provide additional constraints on, and more detailed models of, crustal structure for both profiles. The results of this work will be published in separate papers. However, preliminary results for line 36 are consistent with the gravity modelling results described below.

## *Line BAS967-34*

The total range of free-air anomalies observed along line 34 is >260 mGal. An interesting characteristic of the observed profile along this line is that there is no peak in free-air anomaly associated with the topography of the arc, which suggests that the topography is perfectly compensated by a crustal root. However, this line crosses the deepest saddle in the arc, and regional free-air anomaly maps show large positive free-air anomalies centred on each of the South Sandwich Islands (Livermore *et al.* 1994; Vanneste & Larter 2002).

Gravity and bathymetry data along line 34 used in two-dimensional gravity modelling were

projected on to a line trending 085°. As this direction is nearly perpendicular to both the trench and the arc we consider that errors related to the two-dimensional assumption will be insignificant on this line. Our initial model for line 34, based on the assumptions that the crust on the South American Plate is 7 km thick and the mantle density is uniform, shows the Moho beneath the crest of the arc at a depth of 26.1 km (Fig. 13a). As the seafloor depth over the crest of the arc on this line is 2.4 km, the thickness of arc crust in the model is 23.7 km. However, the back-arc crust in the same model is 14.4 km thick, which seems implausible for reasons outlined above. When the additional assumption was made that the back-arc crust is 7 km thick and the density of the underlying mantle was reduced to match the regional anomaly trend, the modelled crustal thickness beneath the arc decreased to 17.7 km (Fig. 13b). Inclusion of sediments observed on the MCS line in the model resulted in the thickness of the arc crust, including the sediment thickness, being reduced further to 17.3 km (Fig. 13c).

One surprising feature of the model in Figure 13c is that it shows the forearc crust as being even thinner than normal oceanic crust. This is probably a consequence of the fact that a uniform density has been used for the entire mantle to the west of the subducting crust. In reality there will be a gradient of increasing mantle density towards the slab due to its cooling effect. Furthermore, the mantle directly beneath the forearc is probably cooler and denser than most of the mantle wedge because it is most distant from the main flux of the corner flow that is predicted to take place above subducting slabs (Davies & Stevenson 1991; Winder & Peacock 2001). Assuming that a denser mantle beneath the forearc would result in a greater modelled thickness of crust in this area.

The main difficulty encountered in extending subduction-zone gravity models to greater depth is how to represent the transformation of igneous oceanic crust to eclogite. This change is thought to take place at a depth between 40 and 80 km, the precise depth probably being dependent on temperature and water pressure (Ahrens & Schubert 1975; Anderson *et al.* 1976; Delany & Helgeson 1978). In the model shown in Figure 13d this boundary was placed at a depth of 60 km and a density of 3.55 Mg $m^{-3}$ was assigned to the eclogite layer. Before the eclogite body was added, extending of the model to 150 km depth and increasing the mantle density beneath the arc and back-arc had resulted in a decrease in calculated anomaly over the arc, relative to the back-arc, by about 20 mGal. Inserting the eclogite body contributed an additional, broad positive anomaly approximately centred on the arc with amplitude about 55 mGal. Thus, the net effect of extending the model to 150 km depth was a positive residual anomaly of about +35 mGal centred over the arc. In the model shown in Figure 13d, the thickness of the arc crust was increased to eliminate this residual anomaly. The crust beneath the crest of the arc was increased in thickness by 2.7 km to 20.0 km, and the thickness of the crust on both flanks of the arc was increased by smaller amounts. In view of the fact that the densities used for both average arc crust and sediments are towards the high end of the acceptable range, we consider that this model constrains the crustal thickness beneath the crest of the arc on line 34 to be no greater than 20 km.

The effect of the transformation of igneous oceanic crust to eclogite has probably been slightly overestimated in the modelling exercise described above, because no reduction in the thickness of the layer of subducted crust was made to allow for the >20% increase in density. The effect of this overestimation will be to bias the model further towards including thicker arc crust. In reality an eclogite layer may persist deeper than 150 km, but extending the model to greater depth would have very little effect on the crustal section because any density contrast at such great depth would produce a very long wavelength anomaly.

The top of the slab in Figure 13d is at a depth of 90 km beneath the crest of the arc. An alternative model with an increased slab dip was produced, so that the top of the slab was at 110 km depth beneath the arc. This change produced a residual anomaly of about −15 mGal centred over the western flank of the arc. It was found that this residual anomaly could be eliminated by reducing the thickness of the crust on the western flank of the arc by about 1 km, and without any change to the Moho beneath the crest of the arc.

In modifying the model in Figure 13b to produce the model in Figure 13c, the outer forearc material above the reflection at 6.8 s TWT (Fig. 9) was interpreted as sediment and assigned a density of 2.2 Mg $m^{-3}$. The thin layer of sediment over the steepest part of the slope and a small frontal prism were included in a continuation of this body towards the trench. Even after introduction of this body there remained a substantial positive residual anomaly over the lower forearc and trench. We found that the residual anomaly over the outer forearc could be accounted for by reducing the density of the main part of the outer forearc crust to 2.5

Mg $m^{-3}$. However, it was not possible to account for the entire residual anomaly over the trench, and the fact that the calculated anomaly over the eastern flank of the trench has a lower gradient than the observed anomaly, by changes to the outer forearc alone. This problem was not apparent in a gravity model for a nearby profile presented by Vanneste & Larter (2002) because that profile only extended about 25 km east of the trench.

Sager (1980) observed a similar kind of discrepancy on a profile across the Mariana Trench and arbitrarily reduced the crustal thickness beneath the outer rise to make the calculated and observed anomalies match over that part of the profile. In our model we found it would be necessary to make the crustal thickness between the outer rise and the trench differ by more than 6 km if the difference in calculated and observed anomaly was to be explained by this means alone. Instead, we chose to keep the thickness of the oceanic crust constant in the models in Figure 13c and d, and accounted for the difference by introducing a new body with a lower density in the upper part of the crust. It was found to be possible to account for the observed anomaly by making this body 2.5 km thick beneath the trench and reducing its density to 2.5 Mg $m^{-3}$.

### *Line BAS967-36*

The total range of free-air anomalies observed along line 36 is 230 mGal. This range is smaller than on line 34 mainly because the trench is shallower. On this line, which passes close to Southern Thule, there is a free-air anomaly high over the crest of the arc with amplitude +30 mGal relative to the back-arc basin. An interesting characteristic of the observed profile along this line is that the deepest negative anomaly lies about 35 km west of the trench axis, suggesting the presence of a large mass deficit beneath the outer forearc.

Gravity and bathymetry data along line 36 used in two-dimensional gravity modelling were projected on to a line trending 105° . This direction is nearly perpendicular to the trench and forearc high, but the strike of the arc is about 25° clockwise from perpendicular to the projected line. As a result, the positive anomaly associated with the arc will be broader along the projected profile than it would be if the arc were perpendicular to the line. The effect of this on the two-dimensional gravity models in Figure 14 will be to smooth out the Moho relief beneath the arc, with the modelled crust being fractionally too thin beneath the crest of the arc and too thick beneath the flanks of the arc. However, a three-dimensional effect that is probably more significant is the large positive free-air anomaly centred on Southern Thule. The peak of the anomaly is >120 mGal relative to the back-arc region (see fig. 2 in Vanneste & Larter 2002), and line 36 approaches within 12 km of this island group (Fig. 1), cutting across the distal part of the anomaly. The effect of this on the models in Figure 14 will be to make the modelled arc crust slightly too thin, as additional shallow subarc mantle is required to simulate the gravity effect of a mass that is out of the plane of the section. However, even if the entire +30 mGal anomaly over the arc, relative to the back-arc basin, were an out-of-plane effect, the amount by which the models in Figure 14 underestimate the thickness of the arc crust would be <2.5 km.

Our simplest model for line 36, based on the assumptions described above, shows the Moho beneath the crest of the arc at a depth of 24.2 km (Fig. 14a). As the seafloor depth over the crest of the arc on this line is 1.3 km, this is a crustal thickness of 22.9 km. However, once again, the back-arc crust in this model is implausibly thick (13.9 km). When the additional assumption was made that the back-arc crust is 7 km thick and the density of the underlying mantle was reduced to match the regional anomaly trend, the modelled crustal thickness beneath the arc decreased to 18.3 km (Fig. 14b).

An additional change in the model shown in Figure 14b is that the mantle to the east of the trench has been divided into two bodies. This change was made in order to match the observed free-air anomaly gradient on the eastern flank of the trench, which is less steep than the calculated anomaly in Figure 14a. We suspect that this discrepancy is a consequence of lateral density variation being significant in the young oceanic lithosphere approaching the trench here. This variation was simulated by dividing the mantle into two bodies along a boundary that lies approximately along the 1000°C isotherm predicted by a cooling-plate model (Parsons & Sclater 1977).

Inclusion of sediments observed on the MCS line in the model resulted in the thickness of the crust beneath the crest of the arc, including the sediment thickness, being reduced to 13.0 km (Fig. 14c). In this model the body representing the deeper part of the forearc basin (body 9 in Fig. 14c) was continued across the crest of the arc. The MCS data do not show a distinct western boundary to the basin, and if the body was terminated east of the arc crest then even more extreme Moho topography than that in Figure 14c would be needed to cancel out the

gravity effect from such a boundary. The thin (<200 m) and patchy sediments on the outer rise were not included in the model as their effect would be insignificant.

In modifying the model in Figure 14b to produce the model in Figure 14c, the stratified sediments on top of the large fault block, the outer slope sediments and the frontal prism observed on the MCS data were represented by a single body with a density of 2.2 Mg $m^{-3}$ (body 8). Even after introduction of this body there remained a substantial positive residual anomaly over the lower forearc and trench. We found that the residual anomaly over the outer forearc could be accounted for by reducing the density of the main part of the outer forearc crust to 2.45 Mg $m^{-3}$.

A model for line 36 extended to 150 km depth, and with the subducted oceanic crust below 60 km depth replaced by eclogite, is shown in Figure 14d. The two-layer South American mantle used in the 50 km-depth models (Fig. 14b, c) to simulate lateral density variation in the young oceanic lithosphere presented an additional difficulty when increasing the basal depth of the model. An unrealistically low density (3.2 Mg $m^{-3}$) had been used for the deeper of the two mantle bodies as a crude way of approximating a density contrast that extends to greater depth. Simply extending this body to 150 km depth would add a large volume of mantle with an unrealistically low density to the eastern end of the model. Instead, the density of this body was increased to 3.25 Mg $m^{-3}$ and that of the shallower mantle body was increased to 3.35 Mg $m^{-3}$, thus preserving the density contrast between them. After making these changes and extending the model to 150 km depth it was found necessary to increase the density of the mantle body beneath the back-arc and arc to 3.244 Mg $m^{-3}$ to match the observed regional anomaly trend.

Extending of the model to 150 km depth and increasing the mantle densities as described above resulted in a decrease in calculated anomaly over the arc, relative to the back-arc, by about 15 mGal. Inserting the eclogite body contributed an additional, broad positive anomaly approximately centred on the arc with amplitude about 60 mGal. Thus, the net effect of extending the model to 150 km depth was a positive residual anomaly of about +45 mGal centred over the arc. In the model shown in Figure 14d, the thickness of the arc crust was increased and some changes were made to the outer forearc structure to eliminate this residual anomaly. The crust beneath the crest of the arc was increased in thickness by 3.7 km to 16.7 km, and the thickness of the crust on both flanks of the arc was increased by smaller amounts. As explained above, non-two-dimensional effects resulting from the proximity of the line to Southern Thule could mean the arc crust is up to 2.5 km thicker than this. Therefore, in view of the fact that the densities used for both average arc crust and sediments are towards the high end of the acceptable range and, as explained previously, the effect of the transformation of igneous oceanic crust to eclogite has probably been slightly overestimated, we consider that this model constrains the crustal thickness beneath the crest of the arc on line 36 to be no greater than 19.2 km. This is consistent with preliminary results from modelling wide-angle seismic data recorded along this line, which have been interpreted as indicating a maximum crustal thickness of 15 km beneath the arc crest (Larter *et al.* 2001).

## Discussion

Detailed analysis of marine magnetic profiles confirms that organized back-arc spreading in the East Scotia Sea started at least 15 Ma ago, making it the world's longest-lived extant back-arc basin. The back-arc spreading ridge 15 Ma ago was already more than 350 km long (Fig. 1), and spreading has continued to the present day without any detectable ridge jumps. The stability of this spreading regime has probably been facilitated by the stability of motions of the surrounding major plates during this period (Barker & Lawver 1988). The fact that the South Sandwich subduction system has not interacted with any other subduction systems, or encountered features such as aseismic ridges or oceanic plateaux, has probably also been important in contributing to the longevity of the back-arc spreading regime.

The cause for the start of East Scotia Sea extension may have been a change in the direction of South American–Antarctic relative motion, from 120°–300° to the present E–W direction, at about 20 Ma (Barker & Lawver 1988). Drilling results from the western flank of the Lau Basin have been interpreted as evidence of a period of asymmetrical arc rifting that predated organized seafloor spreading (Parson & Hawkins 1994), and extension in the East Scotia Sea may have started in a similar way between 20 and 15 Ma ago. Such asymmetrical arc rifting appears to be taking place at the present day in the northern Mariana Trough (Martinez *et al.* 1995; Baker *et al.* 1996) and the Havre Trough (Parson & Wright 1996; Wright *et al.* 1996), and it has been suggested that magnetic lineations

may be developed even in this rifting phase by systematic migration of zones of magmatism across the rift zone (Martinez *et al.* 1995). Arc rifting is therefore a possible explanation for the origin of the crust with unidentified linear magnetic anomalies that lies between about 35° and 37°W, west of anomaly 5B, in the East Scotia Sea (Fig. 5).

Magnetic anomalies in the eastern part of East Scotia Sea indicate that the central part of the South Sandwich arc is built on crust that was formed at the back-arc spreading ridge about 10 Ma ago. The northernmost and southernmost arc islands are situated on even younger back-arc crust. Therefore, no part of the present arc could have existed when organized back-arc spreading began. It is thought that back-arc spreading is usually initiated close to the line of a pre-existing arc (Karig 1971; Taylor & Karner 1983; Taylor 1992). In some cases initial rifting occurs on the forearc side of the volcanic front (Cole *et al.* 1990; Taylor 1992). The only bathymetric highs along the western edge of the East Scotia Sea that might represent substantial remnant arc volcanic edifices are two circular highs about 150 km south of South Georgia (Fig. 1). Hence, if there was a pre-existing arc, it seems likely that initial rifting was on the back-arc side along most of its length.

If back-arc extension was symmetrical following a transition from arc rifting to organized spreading about 15 Ma ago (chron 5B), then the early spreading rates we have measured imply that crust originally formed at the ESR extends about 80 km east of the central part of the present arc. Even if spreading between 15 and 10 Ma ago was highly asymmetrical, with the rate on the eastern flank of the ESR only half of that on the western flank, crust formed on the eastern flank 15 Ma ago must lie more than 40 km east of the central part of the present arc. Any pre-existing arc must have been even farther east relative to the Sandwich Plate. Analyses of peridotites dredged from the trench-slope break 75–85 km ENE of Zavodovski Island suggest that there was indeed a pre-existing arc in such a position. The peridoites have geochemical characteristics that demonstrate they originated as the residue from melting at a ridge, probably the early ESR, and were subsequently modified by interaction with South Sandwich arc magmas (Pearce *et al.* 2000).

The present arc–trench gap of 140–160 km is one of the narrowest among modern subduction systems, so if the pre-existing arc was situated more than 40–80 km east of the present arc it seems likely that a substantial part of the earlier forearc has been removed by subduction erosion. Even if there was no pre-existing arc, it seems improbable that a 350 km-long back-arc spreading ridge could have developed only about 100 km from the trench, so once again substantial subduction erosion is implied. If it is assumed that the arc has retreated by 80 km and that the pre-existing forearc was as wide as the modern forearc, then the average rate of forearc slope retreat over 15 Ma has been 5.3 km $Ma^{-1}$. However, if arc–trench gaps tend to increase with time, as proposed by Dickinson (1973) and Jarrard (1986), then the average rate of forearc slope retreat could have been somewhat slower than the rate calculated by assuming that the slope retreated as far as the arc has (Vanneste & Larter 2002).

Subduction erosion provides a possible explanation for the absence of relict volcanic edifices of the supposed pre-existing arc from the modern forearc. Forearc slope retreat, and steepening of the forearc slope as a result of basal subduction erosion (Clift & MacLeod 1999), may have made such edifices gravitationally unstable so that they collapsed towards the trench. The only large bathymetric and gravity high that lies far enough east in the forearc for it to possibly represent a relict arc volcano is between 58°30′ and 59°S (Fig. 1). The peak of this high is close to where 15 Ma-old back-arc crust would be predicted to lie if back-arc spreading between 15 and 10 Ma was symmetrical, and within 40 km of the edge of such old back-arc crust even if the ratio of west:east asymmetry in spreading rate at the ESR is assumed to have been 2: 1 during this interval. Dredges from the eastern slope of the high yielded calc-alkaline basalts, basaltic andestites and andesites, and K/Ar ages determined on three samples range from 28.5 to 32.8 Ma (Barker 1995). Such old ages close to where back-arc spreading started about 15 Ma ago are surprising, and results from Ar/Ar dating are awaited with interest. However, a possible interpretation based on the published ages is that these dredged samples represent the exhumed deeper parts of a pre-existing arc volcano that had grown in this position over about 15 Ma prior to the start of East Scotia Sea spreading. If Ar/Ar dating confirms the published ages, then these dredges constrain the maximum extent of old back-arc crust beneath the inner forearc. The present elevation of the high is probably related to more recent tectonic processes, similar to those responsible for the uplift of the forearc high observed on line 36 (Vanneste *et al.* 2002), and this may have promoted erosion of the younger parts of a pre-existing volcanic succession.

If a pre-existing arc migrated gradually to the position of the modern arc as a consequence of subduction erosion, it might be expected that relict volcanic edifices would be found on the modern inner forearc. Vanneste & Larter (2002) suggested such edifices could have formed and subsequently been removed as part of a cyclic process of accumulation and denudation on the inner forearc. An alternative possibility is that the arc moved to its present position in a single jump, as appears to have happened in the northern Lesser Antilles during the Miocene (Westbrook & McCann 1986).

If the northern part of the South Sandwich arc moved to its present position in a single jump, this may partly explain why the forearc crust on line 34 is so thin. As already noted, the forearc crust on line 34 is probably not as thin as shown in Figure 13c and d, because these gravity models do not take into account lateral density variation in the mantle wedge. However, Figure 13a shows that, even using the most extreme assumptions, the forearc crust on this line cannot be much thicker than normal oceanic crust. If the arc migrated gradually to its present position, then either the arc magma supply was small prior to 10 Ma or the forearc crust has been thinned by extension. Recent trench-normal extension in this area appears to be restricted to the outer forearc (Vanneste & Larter 2002), but this does not preclude the possibility that the inner forearc may have been extended at an earlier stage in the history of the arc.

The crust on the western side of the back-arc basin that we interpret as being conjugate to the inner forearc basement on this line is anomalously elevated, which suggests that it is thicker than normal back-arc crust (profiles D–D′, E–E′ and F–F′ in Fig. 3). Therefore, the constraint on thickness of the inner forearc crust derived from gravity modelling is evidence in favour of the inner forearc in this area having been extended earlier in the history of the arc. Vanneste & Larter (2002) suggested that the lack of extensional strain indicators in the inner forearc and arc at the present day may be a consequence of the fact that the East Scotia Sea is a mature back-arc basin, and therefore is expected to contribute a substantial ridge-push force to the stress balance. On this basis, extension induced by subduction erosion near the trench might be expected to have affected a wider area of the forearc during earlier stages of development of the East Scotia Sea. Another possible cause of forearc extension distant from the trench is basal subduction erosion, which can cause mid-forearc subsidence and basin formation (e.g. Laursen *et al.* 2002).

The excess volume of the arc crust in Figure 13d compared to normal, 7 km-thick, oceanic crust is about 720 $km^3\ km^{-1}$ along the arc. If this volume has all been added since a jump in the locus of arc magmatism about 10 Ma ago, it represents an arc growth rate of 72 $km^3\ Ma^{-1}$ for each km along the arc. This rate is similar to the rates estimated for the Aleutian and Izu–Bonin arcs by Holbrook *et al.* (1999) based on travel-time inversion of wide-angle seismic data. It should be remembered that the gravity models presented here were constructed based on assumptions designed to constrain the maximum thickness of the crust. Nevertheless, any overestimation of crustal thickness must be offset against the fact that the modelled section crosses the deepest saddle in the arc and therefore does not include representation of the volume of the volcanic edifices around the arc islands, or any three-dimensional crustal root associated with them. Moreover, the errors resulting from these factors are probably small compared to the overall uncertainties in estimates of arc growth rates, so it is interesting that Figure 13d suggests a growth rate within the range calculated for arcs that have been built over a much longer interval.

The gravity models shown in Figure 14c and d suggest that the crust beneath the forearc high on line 36 is of similar thickness to the arc crust on the same line. Assuming symmetrical spreading during the early stages of back-arc opening, we estimate that the crust beneath the forearc high on line 36 has an age of ≤12.5 Ma (chron 5Ar.1r). In view of the age and thickness of the crust beneath the forearc high, it seems possible that the arc front could have been located in this area before moving to its present position. However, the structural setting of the forearc high suggests that its present elevation results from flexural footwall uplift related to trench-normal extension in the outer forearc (Vanneste *et al.* 2002), so we do not consider the high to be simply the eroded root of a former volcanic edifice.

The nature of the intermediate-density bodies (2.43–2.5 $Mg\ m^{-3}$) inferred to form the bulk of the outer forearc crust is uncertain. These densities are too high for the material to be recently accreted ocean-floor sediments. Furthermore, travel-time inversion of wide-angle seismic data indicates a P-wave velocity of 5.1±0.2 $km\ s^{-1}$ for the eastern part of the intermediate-density body on line 36 (N.J. Bruguier pers. comm. 2001). However, the estimated densities are also considerably lower than the average density of the oceanic crust as a whole (2.89 $Mg^{-3}$), and lower even than estimates of the average density of layer 2 of the oceanic crust (in the range

2.64–2.86 Mg $m^{-3}$; Carlson & Raskin 1984). We speculate that these bodies represent igneous crust that has been pervasively fractured and hydrated. The same explanation may also apply to the intermediate-density body that occupies the upper part of the oceanic crust beneath the trench in the models in Figure 13c and d. Faulting resulting from flexure of the oceanic lithosphere as it approaches the trench may allow water to penetrate deep into the crust and oceanic mantle (Peacock 2001).

## Conclusions

Analysis of magnetic data from the western part East Scotia Sea confirms that the present regime of organized back-arc spreading has been active since at least 15 Ma ago. Extension may have been initiated as a result of a change in direction of South American–Antarctic relative motion about 20 Ma ago. On the eastern side of the East Scotia Sea, crust formed at the ESR forms the basement underlying the South Sandwich arc and inner forearc.

Samples dredged from the forearc provide indications of a previous arc that existed before the start of spreading in the East Scotia Sea and was located more than 80 km east of the modern arc on the Sandwich Plate. The proximity of this former arc to the modern trench suggests that substantial subduction erosion has taken place, with the forearc slope retreat rate perhaps being as high as 5.3 km $Ma^{-1}$.

Gravity models constrained by MCS reflection data indicate that the crust beneath the northern forearc cannot be much thicker than normal oceanic crust. This may indicate that the northern part of the arc moved to its present position in a single jump at some time since 10 Ma, rather than migrating gradually. However, alternative explanations for the thin forearc crust are also possible. If it is assumed that the northern part of the present arc has developed since a jump in the locus of arc magmatism 10 Ma ago, the volume of arc crust in the gravity models represents an arc growth rate of 72 $km^3$ $Ma^{-1}$ $km^{-1}$, which is within the range of growth rates estimated for the Aleutian and Izu-Bonin arcs (Holbrook *et al.* 1999). Models for a line across the southernmost part of the forearc indicate that the mid-forearc crust there is of similar thickness to the arc crust, making a stepwise migration of the arc front more plausible in this area. The gravity models indicate that intermediate-density bodies (2.43–2.5 Mg $m^{-3}$) constitute the bulk of the outer forearc crust in both areas, perhaps representing igneous crust that has been pervasively fractured and hydrated.

We thank everyone who participated in the many cruises over the past 33 years from which we have used magnetic and bathymetry data. In particular we thank all those who sailed with us on RRS *James Clark Ross* cruises JR09a (1995) and JR18 (1997). We are grateful to Fernando Martinez, David Scholl and Tim Minshull for constructive reviews.

## References

AHRENS, T.J. & SCHUBERT, G. 1975. Gabbro-eclogite reaction rate and its geophysical significance. *Reviews of Geophysics and Space Physics*, **13**, 383–400.

ANDERSON, R.N., UYEDA, S. & AKIHO, M. 1976. Geophyscial and geochemical constraints at converging plate boundaries – part 1: dehydration in the downgoing slab. *Geophysical Journal of the Royal Astronomical Society*, **44**, 333–357.

BAKER, N., FRYER, P., MARTINEZ, F. & YAMAZAKI, T. 1996. Rifting history of the northern Mariana trough: SeaMARC II and seismic reflection surveys. *Journal of Geophysical Research*, **101**, 11 427–11 455.

BANGS, N.L., SHIPLEY, T.H. & MOORE, G.F. 1996. Elevated fluid pressure and fault zone dilation inferred from seismic models of the northern Barbados Ridge decollement. *Journal of Geophysical Research*, **101**, 627–642.

BARKER, P.F. 1970. Plate tectonics of the Scotia Sea region. *Nature*, **228**, 1293–1296.

BARKER, P.F. 1972. A spreading centre in the East Scotia Sea. *Earth and Planetary Science Letters*, **15**, 123–132.

BARKER, P.F. 1979. The history of ridge-crest offset at the Falkland–Agulhas Fracture Zone from a small-circle geophysical profile. *Geophysical Journal of the Royal Astronomical Society*, **59**, 131–145.

BARKER, P.F. 1995. Tectonic framework of the East Scotia Sea. *In*: TAYLOR, B. (ed.) *Backarc Basins: Tectonics and Magmatism*. Plenum, New York, 281–314.

BARKER, P.F. & HILL, I.A. 1981. Back-arc extension in the Scotia Sea. *Philosophical Transactions of the Royal Society of London*, **A 300**, 249–262.

BARKER, P.F. & LAWVER, L.A. 1988. South American–Antarctic plate motion over the past 50 Myr, and the evolution of the South American–Antarctic ridge. *Geophysical Journal International*, **94**, 377–386.

BARKER, P.F., BARBER, P.L. & KING, E.C. 1984. An early Miocene ridge crest–trench collision on the South Scotia Ridge near 36°W. *Tectonophysics*, **102**, 315–332.

BARTON, C.E. 1996. Revision of the International Geomagnetic Reference Field released. World Wide Web address: http://www.agu.org/eos_elec/95242e.html

BRUGUIER, N.J. & LIVERMORE, R.A. 2001. Enhanced magma supply at the southern East Scotia Ridge: evidence for mantle flow around the subducting slab? *Earth and Planetary Science Letters*, **191**, 129–144.

CANDE, S.C. & KENT, D.V. 1995. Revised calibration of the geomagnetic polarity timescale for the Late Cretaceous and Cenozoic. *Journal of Geophysical Research*, **100**, 6093–6095.

CARLSON, R.L. & RASKIN, G.S. 1984. Density of the ocean crust. *Nature*, **311**, 555–558.

CARLSON, R.L., GANGI, A.F. & SNOW, K.R. 1986. Empirical reflection travel time versus depth and velocity versus depth functions for the deep sea sediment column. *Journal of Geophysical Research*, **91**, 8249–8266.

CHRISTENSEN, N.I. & MOONEY, W.D. 1995. Seismic velocity structure and composition of the continental crust: a global view. *Journal of Geophysical Research*, **100**, 9761–9788.

CLIFT, P.D. & MACLEOD, C.J. 1999. Slow rates of subduction erosion estimated from subsidence and tilting of the Tonga forearc. *Geology*, **27**, 411–414.

COLE, J.W., GRAHAM, I.J. & GIBSON, I.L. 1990. Magmatic evolution of late Cenozoic volcanic rocks of the Lau Ridge, Fiji. *Contributions to Mineralogy and Petrology*, **104**, 540–554.

DAVIES, J.H. & STEVENSON, D.J. 1992. Physical model of source region of subduction zone volcanics. *Journal of Geophysical Research*, **97**, 2037–2070.

DAVIS, D., SUPPE, J. & DAHLEN, F.A. 1983. Mechanics of fold-and-thrust belts and accretionary wedges. *Journal of Geophysical Research*, **88**, 1153–1172.

DELANY, J.M. & HELGESON, H.C. 1978. Calculation of the thermodynamic consequences of dehydration in subducting ocean crust to 100 kb and >800°C. *American Journal of Science*, **278**, 638–686.

DICKINSON, W.R. 1973. Widths of modern arc–trench gaps proportional to past duration of igneous activity in associated magmatic arcs. *Journal of Geophysical Research*, **78**, 3376–3389.

ENGDAHL, R.E., VAN DER HILST, R. & BULAND, R. 1998. Global teleseismic earthquake relocation with improved travel times and procedures for depth determination. *Bulletin of the Seismological Society of America*, **88**, 722–743.

GARDNER, G.H.F., GARDNER, L.W. & GREGORY, A.R. 1974. Formation velocity and density: the diagnostic basics for stratigraphic traps. *Geophysics*, **39**, 770–780.

HAMILTON, E.L. 1979. Sound velocity gradients in marine sediments. *Journal of the Acoustical Society of America*, **65**, 909–922.

HAMILTON, I.W. 1989. *Geophysical investigations of subduction-related processes in the Scotia Sea*. PhD Thesis, University of Birmingham, UK.

HOLBROOK, W.S., LIZARRALDE, D., MCGEARY, S., BANGS, N. & DIEBOLD, J. 1999. Structure and composition of the Aleutian island arc and implications for continental crustal growth. *Geology*, **27**, 31–34.

JARRARD, R.D. 1986. Relations among subduction parameters. *Reviews of Geophysics*, **24**, 217–284.

JULL, M. & KELEMEN, P.B. 2001. On the conditions for lower crustal convective instability. *Journal of Geophysical Research*, **106**, 6423–6446.

KARIG, D.E. 1971. Origin and development of marginal basins in the western Pacific. *Journal of Geophysical Research*, **76**, 2542–2561.

LALLEMAND, S.E., SCHNÜRLE, P. & MALAVIEILLE, J. 1994. Coulomb theory applied to accretionary and nonaccretionary wedges: possible causes for tectonic erosion and/or frontal accretion. *Journal of Geophysical Research*, **99**, 12 033–12 055.

LARTER, R.D., BRUGUIER, N.J. & VANNESTE, L.E. 2001. Structure, composition and evolution of the South Sandwich island arc: implications for rates of arc magmatic growth and subduction erosion. *Eos, Transactions, American Geophyscial Union*, **82**(47), Fall Meeting Supplement, T32D-10.

LARTER, R.D., KING, E.C., LEAT, P.T., READING, A.M., SMELLIE, J.L. & SMYTHE, D.K. 1998. South Sandwich slices reveal much about arc structure, geodynamics, and composition. *Eos, Transactions, American Geophyscial Union*, **79**, 281, 284–285.

LAURSEN, J., SCHOLL, D.W. & VON HUENE, R. 2002. Neotectonic deformation of the central Chile margin: deepwater forearc basin formation in response to hot spot ridge and seamount subduction. *Tectonics*, **21**, 2-1–2-27, 1038, 10.1029/2001TC901023.

LIVERMORE, R. 2003. Back-arc spreading and mantle flow in the East Scotia Sea. *In*: LARTER, R.D. & LEAT, P.T. (eds) *Intra-oceanic Subduction Systems: Tectonics and Magmatic Processes*. Geological Society, London, Special Publications, **219**, 315–331.

LIVERMORE, R.A. & WOOLLETT, R.W. 1993. Seafloor spreading in the Weddell Sea and southwest Atlantic since the Late Cretaceous. *Earth and Planetary Science Letters*, **117**, 475–495.

LIVERMORE, R., CUNNINGHAM, A., VANNESTE, L. & LARTER, R. 1997. Subduction influence on magma supply at the East Scotia Ridge. *Earth and Planetary Science Letters*, **150**, 261–275.

LIVERMORE, R.A., LARTER, R.D., CUNNINGHAM, A.P., VANNESTE, L., HUNTER, R.J. & THE JR09 TEAM 1995. HAWAII-MR1 sonar survey of the East Scotia Ridge. *BRIDGE Newsletter*, **8**, 51–53.

LIVERMORE, R., MCADOO, D. & MARKS, K. 1994. Scotia Sea tectonics from high-resolution satellite gravity. *Earth and Planetary Science Letters*, **123**, 255–268.

LUDWIG, W.J., NAFE, J.E. & DRAKE, C.L. 1970. Seismic refraction. *In*: MAXWELL, A.E. (ed.) *The Sea, Ideas and Observations in the Study of the Seas*. Wiley, New York, 53–84.

MARTINEZ, F. & TAYLOR, B. 2002. Mantle wedge control on back-arc crustal accretion. *Nature*, **416**, 417–420.

MARTINEZ, F. & TAYLOR, B. 2003. Controls on back-arc crustal accretion: insights from the Lau, Manus and Mariana basins. *In*: LARTER, R.D. & LEAT, P.T. (eds) *Intra-oceanic Subduction Systems: Tectonics and Magmatic Processes*. Geological Society, London, Special Publications, **219**, 19–54.

MARTINEZ, F., FRYER, P., BAKER, N.A. & YAMAZAKI, T. 1995. Evolution of backarc rifting: Mariana Trough, 20°–24°N. *Journal of Geophysical Research*, **100**, 3807–3827.

MOORE, G.F., SHIPLEY, T.H., STOOFA, P.L., KARIG, D.E., TAIRA, A., KURAMOTO, H., TOKUYAMA, H. & SUYEHIRO, K. 1990. Structure of the Nankai

Trough accretionary zone from multichannel seismic reflection data. *Journal of Geophysical Research*, **95**, 8753–8765.

PARK, J.-O., TSURO, T., TAKAHASHI, N., HORI, T., KODAIRA, S., NAKANISHI, A., MIURA, S. & KENADA, Y. 2002. A deep strong reflector in the Nankai accretionary wedge from multichannel seismic data: implications for underplating and interseismic shear stress release. *Journal of Geophysical Research*, **107**(B4), ESE3-1–ESE3-17, 2061, 10.1029/2001JB000262.

PARSON, L.M. & HAWKINS, J.W. 1994. Two-stage ridge propagation and the geological history of the Lau backarc basin. *In*: HAWKINS, J.W., PARSON, L.M., ALLAN, J.F. *et al. Proceedings of the Ocean Drilling Program, Scientific Results*, **135**, 819–828.

PARSON, L.M. & WRIGHT, I.C. 1996. The Lau–Havre–Taupo back-arc basin: a southward-propagating, multi-stage evolution from rifting to spreading. *Tectonophysics*, **263**, 1–22.

PARSONS, B. & SCLATER, J.G. 1977. An analysis of the variation of ocean floor bathymetry and heat flow with age. *Journal of Geophysical Research*, **82**, 803–827.

PEACOCK, S.M. 2001. Are the lower planes of double seismic zones caused by serpentine dehydration in subducting oceanic mantle? *Geology*, **29**, 299–302.

PEARCE, J.A., BARKER, P.F., EDWARDS, S.J., PARKINSON, I.J. & LEAT, P.T. 2000. Geochemistry and tectonic significance of peridotites from the South Sandwich arc–basin system, South Atlantic. *Contributions to Mineralogy and Petrology*, **139**, 36–53.

PELAYO, A.M. & WIENS, D.A. 1989. Seismotectonics and relative plate motion in the Scotia Sea region. *Journal of Geophysical Research*, **94**, 7293–7320.

SAGER, W.W. 1980. Mariana arc structure inferred from gravity and seismic data. *Journal of Geophysical Research*, **85**, 5382–5388.

SMITH, W.H.F. & SANDWELL, D.T. 1997. Global sea floor topography from satellite altimetry and ship depth soundings. *Science*, **277**, 1956–1962.

TAYLOR, B. 1992. Rifting and the volcano-tectonic evolution of the Izu–Bonin–Mariana arc. *In*: TAYLOR, B., FUJIOKA, K. *et al. Proceedings of the Ocean Drilling Program, Scientific Results*, **126**, 627–651.

TAYLOR, B. & KARNER, G.D. 1983. On the evolution of marginal basins. *Reviews of Geophysics and Space Physics*, **21**, 1727–1741.

THOMAS, C., LIVERMORE, R. & POLLITZ, F. 2003. Motion of the Scotia Sea plates. *Geophysical Journal International*, in press.

TREHU, A.M. 1975. Depth versus $(age)^{1/2}$: A perspective on mid-ocean rises. *Earth and Planetary Science Letters*, **27**, 287–304.

VANNESTE, L.E. & LARTER, R.D. 2002. Sediment subduction, subduction erosion and strain regime in the northern South Sandwich forearc. *Journal of Geophysical Research*, **107**(B7), EPM5-1–EPM5-24, 2149, 10.1029/2001JB000396.

VANNESTE, L.E., LARTER, R.D. & SMYTHE, D.K. 2002. A slice of intraoceanic arc: insights from the first multichannel seismic reflection profile across the South Sandwich island arc. *Geology*, **30**, 819–822.

WESTBROOK, G.K. & MCCANN, W.R. 1986. Subduction of Atlantic lithosphere beneath the Caribbean. *In*: VOGT, P.R. & TUCHOLKE, B.E. (eds) *The Geology of North America, Volume M, The Western North Atlantic Region*. Geological Society of America, Boulder, Colorado, 341–350.

WESTBROOK, G.K., LADD, J.W., BUHL, P., BANGS, N. & TILEY, G.J. 1988. Cross section of an accretionary wedge: Barbados Ridge complex. *Geology*, **16**, 631–635.

WHITE, R.S., MCKENZIE, D. & O'NIONS, R.K. 1992. Oceanic crustal thickness from seismic measurements and rare earth element inversions. *Journal of Geophysical Research*, **97**, 19 683–19 715.

WINDER, R.O. & PEACOCK, S.M. 2001. Viscous forces acting on subducting lithosphere. *Journal of Geophysical Research*, **106**, 21 937–21 951.

WRIGHT, I.C., PARSON, L.M. & GAMBLE, J.A. 1996. Evolution and interaction of migrating cross-arc volcanism and backarc rifting: an example from the southern Havre Trough (35°20′–37°S). *Journal of Geophysical Research*, **101**, 22 071–22 086.